Mechanisms underlying the cooperation between loss of epithelial polarity and Notch signaling during neoplastic growth in *Drosophila*

Rémi Logeay[1], Charles Géminard[1], Patrice Lassus[2], Miriam Rodríguez-Vázquez[1], Diala Kantar[1], Lisa Héron-Milhavet[1], Bettina Fischer[3], Sarah J. Bray[4], Jacques Colinge[1], and Alexandre Djiane[1]*

[1] IRCM, Inserm, Univ Montpellier, ICM, Montpellier, France

[2] IRCM, Inserm, Univ Montpellier, ICM, CNRS, Montpellier, France

[3] Dept. of Genetics, University of Cambridge, Cambridge, United Kingdom

[4] Dept. of Physiology Development and Neuroscience, University of Cambridge, Cambridge, United Kingdom

*Author for correspondence: IRCM, Inserm U1194
208, rue des Apothicaires
34298 Montpellier, Cedex, France
tel: +33 (0) 411 283 157
email: alexandre.djiane@inserm.fr

KEY WORDS:

Notch signaling, *Drosophila*, epithelial polarity, neoplasia

SUMMARY

Aggressive neoplastic growth can be initiated by a limited number of genetic alterations, such as the well-established cooperation between loss of cell architecture and hyperactive signaling pathways. However, our understanding of how these different alterations interact and influence each other remains very incomplete. Using *Drosophila* paradigms of imaginal wing disc epithelial growth, we have monitored the changes in Notch pathway activity according to the polarity status of cells (*scrib* mutant). We show that the *scrib* mutation impacts the direct transcriptional output of the Notch pathway, without altering the global distribution of Su(H), the Notch dedicated transcription factor. The Notch-dependent neoplasms require however, the action of a group of transcription factors, similar to those previously identified for Ras/*scrib* neoplasm (namely AP-1, Stat92E, Ftz-F1, and bZIP factors), further suggesting the importance of this transcription factor network during neoplastic growth. Finally our work highlights some Notch/*scrib* specificities, in particular the role of the PAR domain containing bZIP transcription factor and Notch direct target Pdp1 for neoplastic growth.

42 **INTRODUCTION**

43 Epithelial cells represent the basic unit of many organs. They are polarized along an
44 apico-basal (A/B) axis, a feature critical for many aspects of their biology. A/B polarity
45 is controlled by the asymmetric segregation of highly conserved protein complexes
46 such as the Scrib/Dlg/Lgl complex (Bilder et al., 2003; Coopman and Djiane, 2016; St
47 Johnston and Ahringer, 2010). The far-reaching effects of A/B polarity is epitomized
48 by the observation that many tumors of epithelial origin exhibit impaired polarity, and
49 that several viral oncoproteins target polarity complexes (Banks et al., 2012; Huang and
50 Muthuswamy, 2010).

51 Studies in human cell lines and in animal models have also suggested a contributing
52 role of polarity alterations to tumor formation. For instance, mutations in the baso-
53 lateral determinant *SCRIB1* have been shown to control proliferation and invasion in
54 MCF-10A human mammary cells (Cordenonsi et al., 2011). Similarly in *Drosophila,*
55 *scrib*, *dlg* or *lgl* mutations, result in multilayered overgrowth of larval epithelial
56 imaginal discs (Bilder et al., 2003; Bunker et al., 2015). However, this uncontrolled
57 growth is at least partly achieved because larvae exhibiting *scrib* mutations fail to
58 undergo proper metamorphosis and imaginal discs grow for an extended period. Indeed,
59 *scrib* mutant cells actually grow slower than wild-type cells and are eliminated by wild-
60 type neighbors (Cordero et al., 2010; Igaki et al., 2009, 2006; Ohsawa et al., 2011).
61 Interestingly, this is reversed when additional mutations are introduced, such as
62 overexpression of the BTB/POZ chromatin remodelers Abrupt or Chinmo (Doggett et
63 al., 2015; Turkel et al., 2013) or the constitutive activation of signaling pathways (e.g.
64 Ras or Notch), converting *scrib* mutant cells into aggressive, invasive and
65 hyperproliferative cells (Brumby and Richardson, 2003; Pagliarini and Xu, 2003).
66 Similar observations have been reported in mouse, where Notch or Ras activation and
67 *Par3* depletion cooperate to generate aggressive neoplasms in mouse mammary glands
68 (McCaffrey et al., 2012; Xue et al., 2013).

69 The Notch pathway is a highly conserved cell-signaling pathway mis-regulated in
70 several cancers (Ntziachristos et al., 2014; Ranganathan et al., 2011). Upon activation,
71 Notch receptors undergo two proteolytic cleavages to release their intra-cellular domain
72 or NICD, which enters the nucleus, binds to the Notch pathway specific transcription
73 factor CSL (Rbpj in mammals; Suppressor of Hairless, Su(H) in *Drosophila*), and
74 converts it from a repressor to an activator to turn on the transcription of specific target

genes (Bray, 2016). These Notch direct target genes differ depending on cell type and account for the variety of outcomes triggered by Notch activity. Increased Notch activity has been associated with several epithelial cancers such as non-small-cell lung carcinomas (Maraver et al., 2012; Ntziachristos et al., 2014), but in animal models, the sole increase in Notch activity either promotes differentiation or only results in benign over-proliferation (hyperplasia) (Brumby and Richardson, 2003; Djiane et al., 2013; Fre et al., 2005; Ho et al., 2015; McCaffrey et al., 2012). However, as mentioned previously, Notch pathway activation cooperates with loss of polarity to generate invasive neoplasms (Brumby and Richardson, 2003; Ho et al., 2015; McCaffrey et al., 2012; Pagliarini and Xu, 2003).

So, while the cooperation between loss of cell architecture and hyperactive signaling pathways is well established, the underlying mechanisms remain poorly understood. It could merely reflect an additive effect where the consequences of both events combine. Alternatively, it could indicate a more profound integration within epithelial cells where these two events impact on each other to generate unique new behaviors. Using *Drosophila* paradigms of imaginal wing disc epithelial growth, we have monitored the changes in Notch pathway activity according to the polarity status of cells and show that epithelial polarity changes directly impact the transcriptional output of the Notch pathway. We further provide evidence that this Notch redirection is not mediated by new genomic binding regions for Su(H), but relies on the cooperation with Su(H) of a combination of transcription factors, such as Stat and basic leucine zipper (bZIP), whose activity is triggered in response to JNK signaling during polarity loss, extending earlier reports on the cooperation between oncogenic Ras and polarity loss (Atkins et al., 2016; Davie et al., 2015; Külshammer et al., 2015; Uhlirova and Bohmann, 2006). Our work highlights in particular the role of the PAR domain containing bZIP transcription factor Pdp1 for Notch-driven neoplastic growth.

RESULTS

Notch activation and scrib mutation cooperate to promote neoplastic growth

In order to gain insights into the mechanisms underlying neoplastic growth, we first characterized the effects of Notch activation and *scrib* mutation mediated epithelial polarity impairment on wing disc growth. Using precisely controlled *Drosophila* larvae culture conditions (crowding and timing), we compared the phenotypes of wild-type (WT), Nicd overexpressing (N), *scrib* mutant (S), and Nicd overexpressing and *scrib* mutant (NS) 3rd instar wing imaginal discs at 6 days after egg laying at 25C. These different paradigms are shown in Figure 1A-D. For clarity, in all figures N will be shown in green, S in red, and NS in blue. Reproducing our previous observations (Djiane et al., 2013), N discs overgrew compared to WT, but remained as monolayered epithelia, and represent a paradigm of hyperplastic-like growth (Fig. 1A&B). S discs were smaller than WT, but grew as unstratified mass of cells. These discs however showed an extensive expression of the JNK signaling target Mmp1 (Fig. 1C), a metallo-protease implicated in the digestion of the extracellular matrix, indicative that *scrib*-cells activate JNK signaling and are prone to invasiveness (Igaki et al., 2006; Uhlirova and Bohmann, 2006). It is noteworthy that S larvae did not pupariate and if left to grow for longer, the S discs ultimately developed as massive overgrowths with very disrupted epithelial polarity, that invaded and fused with neighboring tissues such as other discs (Bilder et al., 2003). Strikingly, NS discs combined aspects of N and S discs. They were overgrown like N discs, but also expressed high levels of Mmp1 like S discs (Fig. 1D). These discs grew as multilayered tissues and were able to invade the surrounding tissues such as haltere discs, and represent therefore a paradigm for neoplastic-like growth.

Neoplastic and hyperplastic discs have different transcriptomes

The context of the *scribble* mutation converts the Notch-based *Drosophila* wing disc hyperplasia into a paradigm of neoplastic growth. While the cooperation between activated Ras and *scrib* mutations has been studied extensively, mainly in the eye imaginal disc (Atkins et al., 2016; Cordero et al., 2010; Davie et al., 2015; Igaki et al., 2009; Katheder et al., 2017; Pagliarini and Xu, 2003; Toggweiler et al., 2016; Wu et

135 al., 2010), less attention has been given to the cooperation between polarity loss and
136 other activated pathways, such as Notch or Hedgehog (Brumby and Richardson, 2003;
137 Pagliarini and Xu, 2003), preventing an evaluation of how general the studies on Ras
138 signaling are to neoplasia development.
139
140 First, we compared the RNA-Seq transcriptomes of the different genetic conditions, to
141 identify the differently expressed genes in N, S, and NS compared to WT controls
142 (using DESeq with adjusted p-value for multiple testing <0.05; Fig. 1E&F and
143 Supplemental Table S1; (Anders and Huber, 2010). The numbers were broadly similar
144 in the different conditions, N (503 up; 663 dw), S (757 up; 1029 dw), and NS (1003 up;
145 991 dw). Semi-quantitative qRT-PCR validated in a subset of genes the transcriptional
146 changes. For instance, *E2f1*, *Sdr*, and *mxc*, were activated only in N discs, while *Act87E*
147 and *Wnt10*, were activated only in NS. In addition, *Ets21C*, *ftz-f1*, and *Atf3* were up-
148 regulated in all conditions (Supplemental Fig. S1A). Comparing these data with
149 previously published transcriptomes on similar or related genetic backgrounds revealed
150 significant overlap, validating our experimental approaches. For instance, 174/503 up-
151 regulated, and 285/663 down-regulated genes in N were also detected in our previous
152 analysis using dual color differential expression arrays (significant overlap p=1.11e-
153 273, hypergeometric test; (Djiane et al., 2013). Similarly, 676/757 up-regulated genes
154 in S were identified in a previous analysis of *scrib* depleted discs (significant overlap
155 p=4.90e-193; (Bunker et al., 2015).
156
157 GO term analysis (p-value < 0.05) confirmed that, as expected from their genetic
158 composition, the N and NS transcriptomes had over-representation for genes in the
159 Notch signaling pathway (GO:0007219) while the NS and S transcriptomes for genes
160 affected by changes in A/B polarity (GO:0045197; GO0019991) (Fig. 1G). This
161 analysis revealed potential common behaviors shared by N and NS, in particular signs
162 of increased proliferation, consistent with the overgrowth phenotypes (e.g. "mitotic
163 cytokinesis" and "mitotic spindle organization"; GO:0000281; GO:0007052), or
164 behaviors shared between NS and S, such as those related to cell migration (e.g. "border
165 follicle cell migration"; GO:0007298) or cellular stress (e.g. "response to starvation"
166 GO:0042594; "response to endoplasmic reticulum stress" GO:0034976) (Fig. 1G).
167 Notably several GO categories were enriched specifically in NS, including "mitotic

168 G1/G2 DNA damage checkpoint" (GO:0031571/GO:0007095), or gluthatione
169 metabolic process (GO:0006749). These results argue that the combined Notch
170 activation and polarity loss promoted the emergence of new cell behaviors and
171 responses, in particular related to DNA damage responses (Fig. 1G).
172
173
174 ***Hyperplasia and neoplasia harbor different Notch direct target networks***
175 This raises the question of how the defects in *Notch* and in *scrib* cooperate to produce
176 these transcriptional consequences. One particularly critical aspect is how the Notch
177 pathway is affected by the *scrib* mutation. Many signaling pathways, such as Ras,
178 branch and act through several transcription factors and/or combine nuclear and
179 cytoplasmic responses, making the analysis of how they are affected by the *scrib*
180 mutation complicated. Since the Notch pathway is extremely direct and since the major,
181 if not unique, output of Notch signaling is transcriptional activation (Bray, 2016), it
182 offers a unique opportunity to investigate how the *scrib* mutation could potentially
183 affect Notch signaling in the NS cooperation. We thus decided to monitor the genes
184 directly activated by Notch and study whether the Notch direct programme (Notch
185 Direct Targets, NDTs) is affected by the *scrib* mutation.
186 Genes that are directly regulated by Notch (NDTs) should have the transcription
187 complex, containing Su(H) bound at their regulatory regions (Djiane et al., 2013). To
188 identify potential NDTs in N and NS, we thus monitored the genomic regions occupied
189 by the Su(H) transcription factor by genome-wide Chromatin Immuno-Precipitation
190 (ChIP) (Fig. 2A; Supplemental Table S2). These overlapped significantly with our
191 previous analysis of Notch induced overgrowth, suggesting that we have captured all
192 the robust regions of Su(H) enrichment.
193
194 Strikingly, there was a strong overlap in the Su(H) bound regions between N and NS
195 conditions: almost all NS Su(H) peaks (416 out of a total of 464) overlap with peaks
196 present in N discs. This implies that the vast majority of Su(H) binding in NS were also
197 present in N (Fig. 2C & S1C). The overlap was also important between N and S peaks
198 (447/554 S peaks overlapping with N peaks; Fig. 2C & S1C). These results suggests
199 that in NS neoplastic discs, a minority of Su(H) peaks represent new binding regions

200 compared to hyperplastic N discs, and that the new NS behaviors are not the
201 consequence of general redistribution of the Notch specific transcription factor Su(H).
202
203 In order to estimate the programs specifically activated by Notch in N and NS, we then
204 intersected the transcriptomic data with the Su(H) ChIP data, considering that
205 upregulated genes located within 20kb of a Su(H) peak were likely NDTs. Using this
206 approach, we identified similar numbers of NDTs in N (176) and NS (174) (Fig. 2A&B,
207 Supplemental Table S3). Again, there was substantial overlap with previous data, with
208 64/176 NDTs in the N condition being identified in our previous study (significant
209 overlap p=5.89e-96, hypergeometric test; (Djiane et al., 2013). When the N and NS
210 scenarios were compared, 68 genes were common to both and thus represent core NDTs
211 in the wing disc overgrowth. However, a significant proportion of NDTs appeared
212 specific for each condition: 108 for N, 106 for NS. Amongst the 106 NS-specific NDTs,
213 23 were also NDTs in S. Indeed, affecting only polarity with the *scrib* mutation already
214 alters the Notch programme (123 NDTs in S). But the difference between N and NS
215 cannot just be explained by this S contribution as it concerns only 23 NDTs, and taking
216 all comparisons into account, 83 genes appear as true NS-specific NDTs (Fig. 2B).
217 Only a minority were associated with new Su(H) binding regions: around the *87E* locus
218 (*yellow-e3, yellow-e, Ir87a,* and *Act87E*), and the *94A* locus (*CG18596, CG7059,*
219 *CG13857,* and *CG13850*), but also next to the *vito*, *cdi*, and *REG* genes (see
220 Supplemental Table S3).
221 These results indicate that while a core Notch response can be identified in overgrowing
222 wing discs (68 genes; Fig. 2B), the loss of polarity affected the direct transcriptional
223 output of the Notch signaling pathway: 108 NDTs specific to N were lost, while 83
224 NDTs specific to NS were gained. Importantly these changes in the Notch program are
225 only marginally mediated by a redeployment of the Su(H) transcription factor: 11/83
226 NS NDTs correspond to NS-specific Su(H) enrichment.
227
228
229 ***Neoplastic overgrowth is not mediated by the new NS-specific Su(H) regions***
230 Using the NDT datasets, we sought to identify the factors that are required for the
231 transition from N hyperplastic to NS neoplastic growth.

232 First, we decided to investigate the contribution of the DNA damage response. Indeed
233 several NS-specific NDTs are implicated in DNA damage response (e.g. *p53*, *His2Av*)
234 and the GO analysis highlighted categories specific to NS related to "response to
235 oxidative stress" (GO:0006979), "cellular response to gamma radiation"
236 (GO:0071480), and "DNA damage checkpoints" (GO:0031571/0007095). We thus
237 asked whether interfering with such pathways could block the growth and invasiveness
238 of NS tissues. To perform these genetic tests, we generated a stable fly line which
239 overexpressed *Nicd* and *scribRNAi* together with a *GFP* marker under the *Bx-Gal4*
240 driver (driving expression in the pouch of the larval wing discs; *Bx>NS*), and monitored
241 the size of the overgrowth (GFP positive tissue), and its invasiveness potential (Mmp1
242 expressing cells; Fig. 4A).
243 Blocking the oxidative stress response by overexpressing the Reactive Oxygen Species
244 (ROS) sponge CAT and SOD, did not have any significant effect on the NS overgrowth
245 or the expression of Mmp1 (Fig. 4E&F). Similarly, expression of RNAi or dominant
246 negative forms of the severe DNA damage major effector and NS specific NDT *p53*
247 could not modify the NS overgrowth phenotype (Fig. 4E&F). While we cannot exclude
248 that the tools used here were not strong enough, these results suggest that even though
249 activated in NS tissues, oxidative stress and p53-mediated DNA damage responses
250 were either not required to fuel NS growth, or that they could compensate for each other
251 converging ultimately on an as yet unidentified core response promoting NS growth.
252
253 Second, we turned our attention to the NS specific NDTs associated with unique Su(H)
254 binding. Indeed, even though the emergence of new Su(H) binding is not the main
255 mechanism driving the NS-specific Notch programme, it remains possible that these
256 loci and the genes associated are functionally important for the NS neoplastic behavior.
257 We thus asked whether interfering with these 11 specific NS NDTs could block the
258 growth and invasiveness. Knocking down by RNAi the expression of the different
259 genes associated with the *87E* locus (*yellow-e3, yellow-e, Ir87a,* and *Act87E*), and with
260 the *94A* locus (*CG18596, CG7059, CG13857,* and *CG13850*) did not have any
261 significant effect on the NS overgrowth. Similarly, we could not detect any change in
262 NS tumor overgrowth after RNAi-mediated knock-down for *cdi*, *REG,* and *vito* (data
263 not shown). It should be noted however that for several genes only one RNAi could be
264 tested with the potential caveat of insufficient knock-down efficiencies (Xia et al.,

265 2021). However, our results suggest that these NS-specific Su(H) NDTs are not
266 required, at least individually, for NS overgrowth. But even though not strictly required,
267 their overexpression, might still contribute, redundantly with other factors, to the
268 overall NS neoplastic behaviors. Amongst these particular NS NDTs, *Act87E,*
269 associated with the new Su(H) peak at locus *87E* (Fig. 2D) was the most robustly up-
270 regulated in NS (see Supplemental Table S1 & Fig. S1A). When overexpressed in wild-
271 type wing disc, or in combination with activated Notch, Act87E led to robust expression
272 of the metalloprotease and JNK target Mmp1, and cell delamination. Act87E also
273 induced robust expression of the effector caspase Dcp-1 caspase (Supplemental Fig.
274 S2). *Act87E*, might thus represent a stress gene activated in NS initiating cell
275 delamination and ultimately cell death, but whose role is not necessary and/or
276 redundant with other NS-activated genes.
277
278
279 ***Identification of the transcriptional networks in the different growth paradigms***
280 Taken together our results indicate that even though the *scrib* mutation was able to
281 change the transcriptional output of the Notch pathway, the difference between N and
282 NS is not due to a redeployment of Su(H) to activate new NS-specific genes. Other
283 factors brought upon the *scrib* mutation must thus influence gene expression.
284 We thus sought to identify transcriptional factors that could account for the cooperation
285 between Notch and polarity loss. We used the iRegulon software (Janky et al., 2014;
286 Verfaillie et al., 2015) to identify the transcription factors likely co-regulating the genes
287 identified in N, S, or NS. Previous usage of iRegulon on *RasV12/scrib-* overgrown 3rd
288 instar larval discs, highlighted an "oncogenic module" comprising of the Hippo
289 pathway terminal effectors Yki/Sd, the JNK pathway regulated AP-1 factors (in
290 particular Atf3, Kay, and CEBPG), the Jak/Stat pathway, Myc, Crp, and Ftz-F1, (Atkins
291 et al., 2016; Davie et al., 2015; Külshammer et al., 2015).
292
293 Implementing iRegulon on our step-wise Notch-based paradigms allowed us (i) to
294 identify transcriptional modules unique or shared between polarity loss only (S),
295 proliferation only (N), and proliferation plus invasiveness (NS), and (ii) to assess the
296 conservation of the "oncogenic module" identified previously with Ras in a Notch-
297 driven neoplastic paradigm. We performed these analyses feeding iRegulon either with

298 the lists of up-regulated genes in N, S, and NS (Fig. 3 & Supplemental Table S4) or
299 with the lists of NDTs (Fig. S3 & Supplemental Table S5). We decided to focus our
300 analyses on the up-regulated genes here since the overexpressed Nicd triggers
301 transcriptional activation (Bray, 2016) and down-regulated genes might thus represent
302 very indirect effects of the cooperation. Modules identified are presented as Venn
303 diagrams (Fig. 3&S3) highlighting the common and specific transcription factor
304 modules that were identified as likely master regulators of the transcriptional changes
305 in the different conditions. Feeding either up-regulated genes (Fig. 3) or NDTs (Fig.
306 S3) identified similar modules indicating that the Notch pathway condition-specific
307 transcription programs are mediated, at least in part, by transcription factors that
308 broadly affect the whole transcriptome. This is likely also true for other neoplastic
309 paradigms such as Ras, even though this remains to be established. Importantly,
310 iRegulon identified the Notch pathway dedicated transcription factor Su(H) in the N
311 and NS transcriptomes.
312
313 First, focusing on NS, which most resembles the *RasV12/scrib-* paradigms, our analysis
314 identified the same major nodes and the transcription factors associated with the
315 "oncogenic module" as described previously for the *RasV12/scrib-* models:
316 - AP-1 basic Leucine Zipper factors related to stress kinase signaling
317 - Stat92E of the Jak/Stat pathway
318 - Ftz-F1 nuclear receptor
319 - basic Helix-Loop-Helix factors of the Myc family.
320 In NS transcriptome, we also identified a contribution of the E(spl) bHLH
321 transcriptional repressors. *E(spl)-HLH* genes are canonical Notch targets, and they are
322 robustly up-regulated in N and NS, in particular *E(spl)mγ-HLH*.
323
324 The iRegulon analyses also suggested that the AP-1 bZIP, and the Stat92E signatures
325 in NS are contributed by S, since they are also detected in the S transcriptomes, while
326 the Su(H) signature is contributed by N. Finally, iRegulon identified a signature for the
327 Polycomb chromatin silencers specifically in N. Such factors include Pho, a zinc finger
328 protein which binds to Polycomb Responsive Elements (PREs) and recruits Polycomb
329 complexes, and the three Polycomb Repressor Complex 1 components Psc, Su(z)2, and
330 l(3)73Ah. Recently, PRC1 has been associated with specific and unexpected

331 transcriptional activation at larval stages, raising the possibility that in N, such genes,
332 normally repressed at embryonic stages, become active (Loubiere et al., 2020).
333 However, the exact contribution of Polycomb factors, and whether they are actually
334 involved in gene activation upon Notch activation, or whether the "Polycomb" module
335 of iRegulon merely indicates gene de-repression, has not been addressed formally in
336 this study.
337
338
339 ***A polarity-loss response required for NS***
340 In order to validate the functional relevance of the transcription factors identified in the
341 Notch-driven neoplastic growth, we then asked whether their depletion by RNAi could
342 alter the growth and invasiveness of the NS tissue, using the *Bx>NS* fly line described
343 previously. We first focused our analysis on the factors associated with the "oncogenic
344 module".
345
346 We confirmed earlier reports that blocking JNK activity by the overexpression of a JNK
347 dominant negative construct, strongly abolishes NS driven growth (GFP positive tissue
348 size; Fig. 4B&E) and invasiveness (Mmp1 expression; Fig. 4B&F). As shown in the
349 *RasV12/scrib-* paradigms, RNAi mediated knock-down of the Jak/Stat pathway
350 terminal transcription factor *stat92E*, and to a lesser extent *ftz-f1* (Atkins et al., 2016;
351 Davie et al., 2015; Külshammer et al., 2015; Toggweiler et al., 2016) strongly
352 suppressed both growth (GFP) and invasiveness (Mmp1; Fig. 4E&F). Unlike the
353 RasV12 models, we did not identify in the different iRegulon analyses of the N, S, and
354 NS transcriptomes, any particular enrichment for Sd/TEAD, the transcriptional factor
355 mediating the effect of Yki and of the Hippo pathway mediated growth in wing discs.
356 However, impairing Yki activity (through RNAi-mediated knock-down) strongly
357 suppressed NS neoplastic behaviors (Fig. 4C,E&F).
358
359 Taken together these results suggest that independently of the oncogenic driver, Ras or
360 Notch, relatively similar tumorous transcriptional networks (AP-1/Yki/Stat/Ftz-f1) are
361 put in place during their cooperation with polarity loss (Atkins et al., 2016; Davie et al.,
362 2015; Hamaratoglu and Atkins, 2020; Külshammer et al., 2015). Given that these nodes
363 were also identified in the S transcriptome, we suggest that they represent a polarity

364 loss module cooperating with oncogenic signaling pathways Ras or Notch, and likely
365 other pathways such as Hh as was initially reported (Brumby and Richardson, 2003).
366
367
368 ***The PAR domain containing transcription factor Pdp1 is required for neoplastic***
369 ***growth***
370 A striking feature of the iRegulon analyses was the NS/S JNK module, which contained
371 classic basic leucine zipper (bZIP) transcription factors such as Jun or Fos. These
372 factors are involved in complex homo and hetero-dimers mediating cellular responses
373 to different stresses such as DNA damage, oxidative stress… (Reinke et al., 2013), and
374 their binding specificities remain difficult to tease apart. Atf3 has recently been shown
375 to control the expression of genes involved in the maintenance of epithelial polarity,
376 and to be specifically activated in polarity deficient cells and required in the
377 *RasV12/scrib-* overgrowth model (Atkins et al., 2016; Donohoe et al., 2018). Strikingly,
378 amongst the different bZIP predicted by iRegulon to control the NS transcriptome,
379 *Pdp1* is a direct Notch target (common in N, S, and NS; Supplemental Table S3 & Fig.
380 S4A), raising the interesting prospect that Pdp1 could act as feedforward factor to
381 promote neoplastic growth downstream of Notch.
382 Knocking down *Pdp1* using two independent RNAi lines, using the *Bx>NS* fly line, led
383 to a robust reduction of tissue growth (as measured by total GFP area; Fig. 4D&E), and
384 to a reduction in the intensity of Mmp1 staining (Fig. 4D&F). Pdp1 (the homologue of
385 Hepatic Leukemia Factor - HLF) has previously been linked to mitotic cell cycle and
386 growth (Reddy et al., 2006), and shown in the *RasV12/scrib-* paradigms to have only
387 modest effects on invasion, but none on growth. In the context of Notch (*Nicd/scrib-*),
388 the role of *Pdp1* appeared thus more essential, probably because *Pdp1* is a direct Notch
389 target. But while *Pdp1* was required, was it sufficient to promote NS-like tumors?
390 Overexpression of Pdp1 was sufficient to induce cell delamination and spreading, as
391 evidenced by the increased Mmp1 staining and the spreading of GFP positive cells on
392 the anterior part of the disc (Fig. S4C). Strikingly, the combined overexpressions of
393 Nicd and Pdp1 resulted in high Mmp1 staining and a much wider GFP expression
394 domain (compared to Nicd or Pdp1 alone) indicative of invasive and/or delaminating
395 cells extending anteriorly (Fig. S4C-E). Even though these features reproduce in part
396 some of the NS behaviors, in particular the increased Mmp1 staining, it should be noted

397 that the discs overexpressing both Nicd and Pdp1 appeared to grow poorly, unlike NS
398 discs. Furthermore the Mmp1 upregulation upon Nicd&Pdp1 overexpression was not
399 restricted to the overexpressing cells, suggesting that the combination of Nicd and Pdp1
400 in a restricted number of cells (under the control of the *Dpp-Gal4* driver) had non-
401 autonomous effects both on growth and on Mmp1 expression (Fig. S4E, yellow
402 arrowhead). Taken together, these results highlight the important role of Pdp1 in Notch-
403 driven neoplasia (necessity), but show that the sole overexpression of Pdp1 in
404 combination with Nicd is not sufficient for optimal growth as observed in NS tumors,
405 suggesting that the development of NS tumors rely on specific levels of Pdp1, together
406 with the involvement of other transcription factors (e.g. Stat92E, Ftz-f1…).
407

408 **DISCUSSION**

409 In this study, using Notch-driven paradigms of epithelial overgrowth in *Drosophila*
410 wing discs, we describe the molecular mechanisms underlying the cooperation between
411 Notch and polarity loss during neoplasia. We show that epithelial polarity alterations
412 redirect the transcriptional outcome of the Notch signaling pathway, thus defining a
413 specific set of new neoplastic Notch direct targets. We further show that this redirection
414 occurs mainly on pre-existing Su(H) bound regions rather than new ones. Finally, we
415 show that similarly to what was previously described for Ras signaling (Atkins et al.,
416 2016; Davie et al., 2015), the AP-1/Stat/Yki/Ftz-f1 transcription factors are required
417 for the cooperation between Notch signaling and polarity loss during neoplastic growth.
418

419 While cancer genomes exhibit multiple mutations in cancer cells, their functional
420 interactions remain difficult to monitor and model. Neoplastic tissues, generated upon
421 the combination of Notch pathway activation and polarity loss through *scrib* mutation,
422 experience many cellular stresses: DNA damage responses, but also ER and unfolded
423 protein response, starvation, or oxidative stresses. However, even though present, these
424 different stresses and in particular oxidative stress and DNA damage are not
425 individually necessary in the context of polarity loss as blocking them or the cellular
426 response they promote (CAT/SOD overexpression, or inhibition of p53) could not
427 significantly suppress the NS tumorous behaviors. These observations suggest that the
428 different stress pathways activated during polarity loss are either not required for
429 fueling growth (they are rather a consequence than a cause of neoplastic growth), or
430 might act "redundantly" to activate a common core response required for increased
431 growth.
432

433 While *Drosophila* and mouse models have demonstrated that overactive signaling
434 pathways cooperate with epithelial polarity impairment to generate neoplastic growth
435 (Brumby and Richardson, 2003; McCaffrey et al., 2012; Pagliarini and Xu, 2003; Xue
436 et al., 2013), the vast majority of studies seeking to understand the underlying
437 mechanisms, have focused primarily on the cooperation between activated RasV12 and
438 *scrib* mutants, especially in *Drosophila* (Atkins et al., 2016; Cordero et al., 2010; Davie
439 et al., 2015; Igaki et al., 2009; Katheder et al., 2017; Pagliarini and Xu, 2003;
440 Toggweiler et al., 2016; Wu et al., 2010). Importantly, the current study, investigating

441 the cooperation between Notch and polarity, shows that many observations made for
442 Ras can be extended to Notch, suggesting that the paradigms used are not a Ras
443 specificity but might represent a more general tumor growth paradigm. But, since the
444 main, if not only, Notch pathway outcome is transcriptional, the *Nicd/scrib-* model
445 allowed to study in greater details the modes of cooperation. The cooperation between
446 Notch pathway activation and polarity loss led to a specific transcriptional programme,
447 and in particular the activation of new Notch direct targets. We could show that this
448 was not the consequence of a general redeployment to new target genes loci of Su(H),
449 the Notch pathway-dedicated transcription factor, ruling-out one possible model for the
450 oncogene/polarity cooperation. What could thus be the mechanisms controlling which
451 genes were activated in the different conditions? All "Notch" activating transcriptional
452 complexes comprise of Nicd, Mastermind, and Su(H). While no differences in overall
453 levels of Nicd and Su(H) could be detected by western-blot (data not shown), they could
454 be differently modified post-translationally leading to different Notch responses (core
455 Notch response, N-only, NS-only...). Indeed, recent reports point towards different
456 post-translational modifications for Su(H) (Frankenreiter et al., 2021). Whether they
457 lead to different transcriptional programmes, and whether they occur *in vivo* in the N
458 and NS models remain however to be studied. Through the use of iRegulon, we could
459 show that the genes of the NS transcriptome, and most importantly the NS Notch direct
460 targets, were enriched in their regulatory regions for elements corresponding to specific
461 transcription factors, and in particular Stat92E or bZIP factors. The fact that similar
462 transcription factor families were found in the whole up-regulated genes, and in the
463 more limited Notch direct genes, suggest that the Notch out-put was controlled, at least
464 in part, by factors that act more broadly on the genome. These analyses support a model
465 where polarity loss redirects the out-put of the Notch transcriptional programme by the
466 action of cooperating transcription factors. However, further work such as detailed
467 comparative ChIP analyses of the different factors in the different conditions, is
468 required to firmly establish this model.
469
470 Even though we could highlight the involvement of a similar "oncogenic module" as
471 identified for the *RasV12/scrib-* neoplastic model (Atkins et al., 2016; Davie et al.,
472 2015; Külshammer et al., 2015), there are specifics that are likely oncogene specific.
473 First, unlike what was reported for *RasV12/scrib-* transcriptomes, Yki/Sd/TEAD

474 modules were not found enriched in the different *Notch* and *scrib-* transcriptomes. In
475 the case of Ras, it was shown that Yki activity could reprogram Ras by promoting the
476 expression of the Ras pathway specific regulators Capicua and Pointed to promote
477 aggressive growth (Pascual et al., 2017). Both genes were either unaffected (*capicua*)
478 or downregulated (*pointed*) in NS Notch driven neoplastic paradigm, suggesting that,
479 even though Yki is clearly required (Fig. 4C), changes in the expression of capicua and
480 pointed are unlikely mediators here. These differing results in the enrichment of
481 Yki/Sd/TEAD motifs between Notch and Ras transcriptomes in the context of polarity
482 loss, might reflect the inhibitory effect Notch has on Yki activity in the wing pouch, in
483 part through the action of the *vestigial* (Djiane et al., 2014). Furthermore, in NS
484 transcriptome, we identified a contribution of the E(spl) bHLH transcriptional
485 repressors, canonical Notch targets (Bray, 2016), which represents thus a Notch
486 specificity. However, the fact that motifs for E(spl)-HLH repressors are found in the
487 up-regulated transcriptome of NS and not N could suggest that in NS, the repressive
488 ability of E(spl)-HLH factors is antagonized, further allowing higher expression of
489 Notch targets. More precisely, our previous work identified many incoherent feed-
490 forward loops in the N hyperplastic transcriptome, including through the action of
491 E(spl) repressors (Djiane et al., 2013), which might thus be resolved in NS. It would be
492 interesting to explore further the link between NS and E(spl)-HLH-mediated
493 repression, but due to the high redundancy between the seven E(spl)-HLH factors
494 (δ, γ, β, 3, 5, 7, 8) and Dpn, the requirement of E(spl)-HLH-mediated repression in the
495 Notch-driven neoplasia could not be formally tested.
496
497 While performing functional assays to identify the genes and processes required for NS
498 tumor growth, we could show that the Notch direct targets associated with "de-novo"
499 NS-specific Su(H) peaks were unlikely to be major contributors. We show however
500 that the bZIP PAR domain containing factor Pdp1 is required for NS tumor growth and
501 invasiveness. Su(H) is bound in the vicinity of Pdp1 in all wing discs set-ups and in
502 particular in N and NS, and Pdp1 represents a "core" Notch target activated in all
503 overgrowth conditions, albeit at higher levels in polarity deficient conditions (Fig.
504 S4A). Pdp1 is not only a Notch target, but also a Jak/Stat target, at least in the
505 developing eye, and canonical tandem Stat92E putative binding sites are found in its
506 second intron, although not overlapping with Su(H) binding which is found in its first

507 intron (Flaherty et al., 2009). Interestingly, Pdp1 is required for Stat92E
508 phosphorylation and efficient Jak/Stat signaling (Baeg et al., 2005), suggesting that
509 Notch might amplify Stat92E signaling during wing disc neoplastic growth, both
510 through ligand expression (Upd ligands are Notch direct targets; this study; (Djiane et
511 al., 2013)), and Pdp1 expression.
512 Even though Pdp1 downregulation could suppress NS neoplastic growth, it was not as
513 efficient as JNK inhibition, or Yki downregulation, suggesting that other factors in
514 parallel to Pdp1 might be involved, such as the previously identified Atf3 (Donohoe et
515 al., 2018), but also the other Notch direct target Ets21C (Fig. 2D; (Külshammer et al.,
516 2015; Toggweiler et al., 2016). Indeed, RNAi-mediated knock down of *Atf3* or *ets21C*
517 partly suppressed *Bx>NS* tumor growth (GFP) and invasiveness (Mmp1; data not
518 shown). This action of both Pdp1 and Ets21C suggest a feedforward loop downstream
519 of Notch that in the context of polarity loss and JNK activity promotes neoplastic
520 growth (Fig. 4G). However, since *Atf3, Pdp1*, and *Ets21C* (but also *Ftz-f1*) are all
521 upregulated in N hyperplastic conditions, their sole upregulation cannot be sufficient
522 for neoplasia. The fact that Atf3 and Pdp1 iRegulon enrichments are not found in N
523 (Fig. 3 and S3), could indicate that despite being upregulated in hyperplastic N, their
524 transcriptional activities are hindered, or that one key cooperating factor enabling their
525 action is missing. Further studies are thus required to test this possibility and study how,
526 in the context of normal epithelial polarity, Notch activation prevents the action of
527 Pdp1/Ets21C/Atf3, thus preventing the transition to neoplasia.
528

529 **MATERIALS AND METHODS**

530 ***Drosophila genetics***

531 The different overgrowth paradigms were obtained by generating random clones in 3rd
532 instar wing discs at high frequency as previously published in (Djiane et al., 2013). In
533 brief, the *abxUbxFLPase; Act>y>Gal4, UAS GFP; FRT82B tubGal80* flies were
534 crossed either to *FRT82B* (to generate Ctrl discs), or to *UAS-Nicd; FRT82B* (to generate
535 hyperplastic N discs), or to *UAS-Nicd; FRT82B scrib1* (to generate neoplastic NS
536 discs). *scrib1* represents a loss of function allele for the *scribble* gene. Because *scrib1*
537 clones are eliminated in growing discs, the dysplasic S discs were obtained from
538 *FRT82B scrib1 / Df(3R)BSC752* 3rd instar larvae. All crosses were performed at 25°C
539 and carefully staged (time after egg laying and tube crowding).

540 For transcriptomic and ChIP analyses, discs were dissected from these carefully timed
541 animals. N, S, and NS overall larval body sizes were very similar to WT controls at day
542 5 and 6, suggesting that they grew normally during 2nd and 3rd instar larval stages. All
543 animals with wing disc growth defects displayed pupariation delay: S and NS never
544 pupate, while some (not all) N animals eventually pupate at day 11 or 12 after egg
545 laying (ael; normal time being 5 to 6 ael). These observations suggest that the main
546 timing problem for N, S, and NS was in the transition to pupa at 5 to 6 ael. By
547 monitoring differences at day 6 ael, just after spiracle eversion (a classic landmark in
548 developmental timing), we thus monitored differences just prior to the extension of
549 larval life, and very far from the extreme that could be observed, suggesting that tissues
550 would remain comparable.

551 For functional studies, neoplastic growth was obtained by driving *UAS-Nicd* and the
552 *scrib* RNAi *P{TRiP.HMS01490}attP2* by the *Bx-Gal4* (pouch of larval wing discs).
553 Modifications of the overgrowth phenotype and of the expression of the Mmp1 invasive
554 marker were performed by crossing in F1 *Bx-Gal4, UAS GFP;; UAS Nicd, UAS*
555 *scribHMS01490* to the desired *UAS RNAi* or control lines (*UAS white RNAi, UAS*
556 *yellow RNAi,* or *UAS GFP*), to ensure similar UAS load. List of lines tested in
557 Supplemental Materials.

558 Information on gene models and functions, and on *Drosophila* lines available were
559 obtained from FlyBase (flybase.org – (Thurmond et al., 2019)).

560

561 ***RNA extraction and RNA-Seq***

562 RNA from 60 or 80 dissected third instar larva wing discs of WT, N, NS and S discs
563 was extracted using TriZOL. Genomic DNA was eliminated using Ambion's DNA-
564 free kit (#AM1906). cDNA bank preparation were then performed from 1µg of RNA
565 and sequencing on a Illumina HisSeq 2000 by the Biocampus genomic facility MGX
566 of Montpellier. After sequencing, reads obtained were filtered based on their quality
567 (circa 40 millions reads were kept per conditions). The reads were then align on
568 *Drosophila* dm6 genome by the ABIC facility in Montpellier producing a matrix of
569 reads per gene and per condition. This matrix was then normalized and pair-wise
570 differential expression was performed using DESeq (Anders and Huber, 2010). Other
571 differential expression tools were tested such as DESeq2 and edgeR with default
572 parameters but appeared either less stringent, or inadequate.
573
574 ***qPCR***
575 qPCR was performed on biological triplicates on a Roche LightCycler 480, and fold
576 change was estimated by the ΔΔCT approach. List of primers used in Supplemental
577 Materials.
578
579 ***Su(H) Chromatin Immuno Precipitation***
580 After dissection in PBS 1X, Protein/DNA complexes from 60 wing discs (80 for S
581 condition) were cross-linked with 1% formaldehyde for 10 minutes. The reaction was
582 then quenched by 0.125 M Glycine and washed 3x in PBS. Wing disc cells were
583 resuspended in 50µL Nuclear Lysis Buffer (Tris-HCl pH 8.1 20mM, EDTA 10mM,
584 SDS 1%). Lysates were sonicated on a Bioruptor (Diagenode), and diluted 10x in
585 Immunoprecipitation Dilution Buffer (Tris-HCl pH 8.1 20mM, EDTA 2mM, SDS
586 0.01%, NaCl 150mM, Triton X-100 1%) and precleared with rabbit IgG (Sigma) and
587 protein G Agarose (Santa Cruz Biotechnology). ChIP reactions were performed by
588 incubating lysates overnight at 4°C with 1ng of Goat anti-Su(H) (Santa Cruz
589 Biotechnology, sc15813), and immunocomplexes were then isolated with Protein G
590 Agarose for 2h, washed 2x with Wash Buffer 1 (Tris-HCl pH 8.1 20mM, EDTA 2mM,
591 SDS 0.1%, NaCl 50mM, Triton X-100 1%) and 2x with Wash Buffer 2 (Tris-HCl pH
592 8.1 10mM, EDTA 1mM, LiCl 250mM, NP-40 1%, Deoxycholic acid 0.4%), before a
593 decross-linking step at 65°C in 0.25M NaCl. Samples were then treated with 0.2 mg/mL
594 proteinase K and 50mg/mL RNase A. The DNA was then purified on columns (Qiagen,

595 28106). ChIP efficiency was checked by qPCR normalized on input chromatin with the
596 following primer couples, corresponding to known strong binding sites of Su(H). List
597 of primers used in Supplemental Materials.
598 For whole-genome analysis, 1 μg double-stranded ChIP or input DNA (corresponding
599 to 180 discs for each replicate) was labelled with either Cy3- or Cy5-random primers
600 using the Nimblegen Dual Colour kit. Both ChIP and input were co-hybridised to
601 NimbleGen D. melanogaster ChIP-chip 2.1 M whole-genome tiling arrays in the
602 NimbleGen hybridisation station at 42°C for 16 h and then washed according to the
603 NimbleGen Wash Buffer kit instructions. The data obtained were normalized using
604 quantile normalization across the replicate arrays in R. Window smoothing and peak
605 calling were performed using the Bioconductor package Ringo (Toedling et al., 2007)
606 with a winHalfSize of 300 bp and min.probes = 5. Probe levels were then assigned P-
607 values based on the normalNull method, corrected for multiple testing using the
608 Hochberg–Benjamini algorithm and then condensed into regions using distCutOff of
609 200 bp.
610 In order to determine the Notch Direct Targets (NDTs), ChIP and RNA-Seq results
611 were compared: NDTs are defined as up-regulated genes with Su(H) enrichment within
612 20kb. As such one Su(H) peak could be assigned to several upregulated genes
613 consistent with its role in enhancer regions. The 20kb window was chosen as it allowed
614 the recovery of more than 85% of NDTs in our previous study that was based on closest
615 gene assignment irrespective of distance (Djiane et al., 2013).
616
617 ***GO Term analyses***
618 The lists of significantly regulated genes in the various comparisons were submitted to
619 gene ontology (GO) term enrichment analysis. We used the GO biological process
620 (GOBP) ontology and applied hypergeometric tests (p-values) followed by Benjamini-
621 Hochberg multiple hypothesis correction (q-values).
622
623 ***iRegulon analyses***
624 In order to determine the likely transcriptional modules in our transcriptomic and NDTs
625 datasets, we used the online tool iRegulon (http://iregulon.aertslab.org/) (Janky et al.,
626 2014; Verfaillie et al., 2015), with the standard settings using the 6K Motif collection
627 (6383 PWMs) and a Putative regulatory region of "10kb upstream, full transcript and

628 10kb downstream". Importantly, these settings allowed the recovery of the "positive
629 control" Su(H) module.
630
631 ***Immunofluorescence***
632 Antibody staining of wing imaginal discs were performed using standard protocols.
633 Briefly, larval heads containing the imaginal discs (LH) were dissected in cold PBS and
634 fixed for 20min in 4% Formaldehyde in PBS at room temperature (RT), before being
635 rinsed 3x 10min in PBS 0.2% TritonX100 (PBT), and blocked in PBT + 0.5% BSA
636 (PBTB) for 30min at RT. LH were then incubated overnight at 4°C with primary
637 antibodies in PBTB. LH were then rinsed 3x 10min in PBT at RT and before being
638 incubated with secondary antibody in PBTB for 90min at RT. LH were then rinsed 3x
639 20min in PBT at RT, before being equilibrated overnight in Citifluor mounting media
640 (Agar). Discs were then further dissected and mounted. Images were acquired on a
641 Zeiss Apotome2 or Leica Thunder microscope and processed and quantified using Zen,
642 Las X, or ImageJ. Primary antibodies used were rabbit anti cleaved Drosophila Dcp-1
643 (9578, Cell Signaling Technologies, 1:200), rat anti-DE-Cadherin (DCAD2,
644 Developmental Studies Hybridoma Bank – DHSB, 1:25), rabbit anti-GFP (A6455,
645 Molecular Probes, 1:200), and mouse anti-Mmp1 (3A6B4, DHSB, 1:25). Secondary
646 antibodies used conjugated to Alexa-350, Alexa-488, or Cy3 were from Jackson Labs
647 Immuno Research (1:200).
648
649 ***Quantification methods***
650 Genotypes were tested in batches with controls and 10-20 images corresponding to 10-
651 20 different discs were all acquired on the same microscope with the same exposure
652 settings.
653 Growth was estimated by the size of the GFP positive area measured as pixel numbers.
654 Mmp1 intensities were ranked as High, Low, Null by independent observer with
655 genotypes masked and processed in random order. Graphs and statistics (indicated in
656 the legends) were performed using the GraphPad Prism software.
657
658 ***Raw data***
659 The data discussed in this publication have been deposited in NCBI's Gene Expression
660 Omnibus (Edgar et al., 2002) and are accessible through GEO Series accession number

GSE185339 (https://www.ncbi.nlm.nih.gov/geo/query/acc.cgi?acc=GSE185339), and GSE185490 (https://www.ncbi.nlm.nih.gov/geo/query/acc.cgi?acc=GSE185490)."

ACKNOWLEDGEMENTS

We thank G. Alvès, D. Andrew, D. Eberl, P. Léopold, R. Levayer, C. Maurange, A. Teleman, J. Terman, and T.T. Su for sharing flies. We acknowledge the Bloomington Stock Center, the Vienna Stock Center, the DGRC Kyoto Stock Center, the Developmental Studies Hybridoma Bank, the *Drosophila* facility, the MGX sequencing facility (BioCampus Montpellier, CNRS, INSERM, Université de Montpellier), and FlyBase for their support to our research.

The lab of SJB is supported by the MRC (MRC programme grant MR/L007177/1). RL was supported by fellowships from "Ligue Nationale Contre le Cancer - LNCC" and from "Fondation ARC pour la recherche sur le cancer". The lab of AD is supported by the "Fondation ARC pour la recherche sur le cancer", "Marie Curie CIG", and "Agence Nationale de la Recherche - ANR-18-CE14-0041".

AUTHOR CONTRIBUTIONS

RL, CG, PL, MRV, DK, and AD performed experiments; RL, CG, LHM, JC, and AD analyzed data; JC provided expertise for RNA-Seq; BF and SJB provided technical support and expertise for ChIP; RL, SJB, and AD wrote the manuscript; AD conceived and supervised the project.

DECLARATION OF INTEREST

The authors declare no competing interests.

688 **REFERENCES**

689 Anders S, Huber W. 2010. Differential expression analysis for sequence count data.
690 *Genome Biol* **11**:R106. doi:10.1186/gb-2010-11-10-r106
691 Atkins M, Potier D, Romanelli L, Jacobs J, Mach J, Hamaratoglu F, Aerts S, Halder G. 2016.
692 An Ectopic Network of Transcription Factors Regulated by Hippo Signaling
693 Drives Growth and Invasion of a Malignant Tumor Model. *Curr Biol* **26**:2101–
694 2113. doi:10.1016/j.cub.2016.06.035
695 Baeg G-H, Zhou R, Perrimon N. 2005. Genome-wide RNAi analysis of JAK/STAT signaling
696 components in Drosophila. *Genes Dev* **19**:1861–1870. doi:10.1101/gad.1320705
697 Banks L, Pim D, Thomas M. 2012. Human tumour viruses and the deregulation of cell
698 polarity in cancer. *Nat Rev Cancer* **12**:877–886. doi:10.1038/nrc3400
699 Bilder D, Schober M, Perrimon N. 2003. Integrated activity of PDZ protein complexes
700 regulates epithelial polarity. *Nat Cell Biol* **5**:53–58. doi:10.1038/ncb897
701 Bray SJ. 2016. Notch signalling in context. *Nat Rev Mol Cell Biol* **17**:722–735.
702 doi:10.1038/nrm.2016.94
703 Brumby AM, Richardson HE. 2003. scribble mutants cooperate with oncogenic Ras or
704 Notch to cause neoplastic overgrowth in Drosophila. *EMBO J* **22**:5769–5779.
705 doi:10.1093/emboj/cdg548
706 Bunker BD, Nellimoottil TT, Boileau RM, Classen AK, Bilder D. 2015. The transcriptional
707 response to tumorigenic polarity loss in Drosophila. *Elife* **4**.
708 doi:10.7554/eLife.03189
709 Coopman P, Djiane A. 2016. Adherens Junction and E-Cadherin complex regulation by
710 epithelial polarity. *Cell Mol Life Sci* **73**:3535–3553. doi:10.1007/s00018-016-
711 2260-8
712 Cordenonsi M, Zanconato F, Azzolin L, Forcato M, Rosato A, Frasson C, Inui M,
713 Montagner M, Parenti AR, Poletti A, Daidone MG, Dupont S, Basso G, Bicciato S,
714 Piccolo S. 2011. The Hippo transducer TAZ confers cancer stem cell-related
715 traits on breast cancer cells. *Cell* **147**:759–772. doi:10.1016/j.cell.2011.09.048
716 Cordero JB, Macagno JP, Stefanatos RK, Strathdee KE, Cagan RL, Vidal M. 2010.
717 Oncogenic Ras diverts a host TNF tumor suppressor activity into tumor
718 promoter. *Dev Cell* **18**:999–1011. doi:10.1016/j.devcel.2010.05.014
719 Davie K, Jacobs J, Atkins M, Potier D, Christiaens V, Halder G, Aerts S. 2015. Discovery of
720 transcription factors and regulatory regions driving in vivo tumor development
721 by ATAC-seq and FAIRE-seq open chromatin profiling. *PLoS Genet* **11**:e1004994.
722 doi:10.1371/journal.pgen.1004994

723 Djiane A, Krejci A, Bernard F, Fexova S, Millen K, Bray SJ. 2013. Dissecting the
724 mechanisms of Notch induced hyperplasia. *EMBO J* **32**:60–71.
725 doi:10.1038/emboj.2012.326
726 Djiane A, Zaessinger S, Babaoğlan AB, Bray SJ. 2014. Notch inhibits Yorkie activity in
727 Drosophila wing discs. *PLoS ONE* **9**:e106211. doi:10.1371/journal.pone.0106211
728 Doggett K, Turkel N, Willoughby LF, Ellul J, Murray MJ, Richardson HE, Brumby AM.
729 2015. BTB-Zinc Finger Oncogenes Are Required for Ras and Notch-Driven
730 Tumorigenesis in Drosophila. *PLoS ONE* **10**:e0132987.
731 doi:10.1371/journal.pone.0132987
732 Donohoe CD, Csordás G, Correia A, Jindra M, Klein C, Habermann B, Uhlirova M. 2018.
733 Atf3 links loss of epithelial polarity to defects in cell differentiation and
734 cytoarchitecture. *PLoS Genet* **14**:e1007241. doi:10.1371/journal.pgen.1007241
735 Edgar R, Domrachev M, Lash AE. 2002. Gene Expression Omnibus: NCBI gene expression
736 and hybridization array data repository. *Nucleic Acids Res* **30**:207–210.
737 doi:10.1093/nar/30.1.207
738 Flaherty MS, Zavadil J, Ekas LA, Bach EA. 2009. Genome-wide expression profiling in the
739 Drosophila eye reveals unexpected repression of notch signaling by the
740 JAK/STAT pathway. *Dev Dyn* **238**:2235–2253. doi:10.1002/dvdy.21989
741 Frankenreiter L, Gahr BM, Schmid H, Zimmermann M, Deichsel S, Hoffmeister P,
742 Turkiewicz A, Borggrefe T, Oswald F, Nagel AC. 2021. Phospho-Site Mutations in
743 Transcription Factor Suppressor of Hairless Impact Notch Signaling Activity
744 During Hematopoiesis in Drosophila. *Front Cell Dev Biol* **9**:658820.
745 doi:10.3389/fcell.2021.658820
746 Fre S, Huyghe M, Mourikis P, Robine S, Louvard D, Artavanis-Tsakonas S. 2005. Notch
747 signals control the fate of immature progenitor cells in the intestine. *Nature*
748 **435**:964–968. doi:10.1038/nature03589
749 Hamaratoglu F, Atkins M. 2020. Rounding up the Usual Suspects: Assessing Yorkie, AP-1,
750 and Stat Coactivation in Tumorigenesis. *Int J Mol Sci* **21**:E4580.
751 doi:10.3390/ijms21134580
752 Ho DM, Pallavi SK, Artavanis-Tsakonas S. 2015. The Notch-mediated hyperplasia
753 circuitry in Drosophila reveals a Src-JNK signaling axis. *Elife* **4**:e05996.
754 doi:10.7554/eLife.05996
755 Huang L, Muthuswamy SK. 2010. Polarity protein alterations in carcinoma: a focus on
756 emerging roles for polarity regulators. *Curr Opin Genet Dev* **20**:41–50.
757 doi:10.1016/j.gde.2009.12.001

758 Igaki T, Pagliarini RA, Xu T. 2006. Loss of cell polarity drives tumor growth and invasion
759 through JNK activation in Drosophila. *Curr Biol* **16**:1139–1146.
760 doi:10.1016/j.cub.2006.04.042
761 Igaki T, Pastor-Pareja JC, Aonuma H, Miura M, Xu T. 2009. Intrinsic tumor suppression
762 and epithelial maintenance by endocytic activation of Eiger/TNF signaling in
763 Drosophila. *Dev Cell* **16**:458–465. doi:10.1016/j.devcel.2009.01.002
764 Janky R, Verfaillie A, Imrichová H, Van de Sande B, Standaert L, Christiaens V,
765 Hulselmans G, Herten K, Naval Sanchez M, Potier D, Svetlichnyy D, Kalender Atak
766 Z, Fiers M, Marine J-C, Aerts S. 2014. iRegulon: from a gene list to a gene
767 regulatory network using large motif and track collections. *PLoS Comput Biol*
768 **10**:e1003731. doi:10.1371/journal.pcbi.1003731
769 Katheder NS, Khezri R, O'Farrell F, Schultz SW, Jain A, Rahman MM, Schink KO,
770 Theodossiou TA, Johansen T, Juhász G, Bilder D, Brech A, Stenmark H, Rusten TE.
771 2017. Microenvironmental autophagy promotes tumour growth. *Nature*
772 **541**:417–420. doi:10.1038/nature20815
773 Külshammer E, Mundorf J, Kilinc M, Frommolt P, Wagle P, Uhlirova M. 2015. Interplay
774 among Drosophila transcription factors Ets21c, Fos and Ftz-F1 drives JNK-
775 mediated tumor malignancy. *Dis Model Mech* **8**:1279–1293.
776 doi:10.1242/dmm.020719
777 Loubiere V, Papadopoulos GL, Szabo Q, Martinez A-M, Cavalli G. 2020. Widespread
778 activation of developmental gene expression characterized by PRC1-dependent
779 chromatin looping. *Sci Adv* **6**:eaax4001. doi:10.1126/sciadv.aax4001
780 Maraver A, Fernández-Marcos PJ, Herranz D, Muñoz-Martin M, Gomez-Lopez G,
781 Cañamero M, Mulero F, Megías D, Sanchez-Carbayo M, Shen J, Sanchez-Cespedes
782 M, Palomero T, Ferrando A, Serrano M. 2012. Therapeutic effect of γ-secretase
783 inhibition in KrasG12V-driven non-small cell lung carcinoma by derepression of
784 DUSP1 and inhibition of ERK. *Cancer Cell* **22**:222–234.
785 doi:10.1016/j.ccr.2012.06.014
786 McCaffrey LM, Montalbano J, Mihai C, Macara IG. 2012. Loss of the Par3 polarity protein
787 promotes breast tumorigenesis and metastasis. *Cancer Cell* **22**:601–614.
788 doi:10.1016/j.ccr.2012.10.003
789 Ntziachristos P, Lim JS, Sage J, Aifantis I. 2014. From fly wings to targeted cancer
790 therapies: a centennial for notch signaling. *Cancer Cell* **25**:318–334.
791 doi:10.1016/j.ccr.2014.02.018

792 Ohsawa S, Sugimura K, Takino K, Xu T, Miyawaki A, Igaki T. 2011. Elimination of
793 oncogenic neighbors by JNK-mediated engulfment in Drosophila. *Dev Cell*
794 **20**:315–328. doi:10.1016/j.devcel.2011.02.007
795 Pagliarini RA, Xu T. 2003. A genetic screen in Drosophila for metastatic behavior. *Science*
796 **302**:1227–1231. doi:10.1126/science.1088474
797 Pascual J, Jacobs J, Sansores-Garcia L, Natarajan M, Zeitlinger J, Aerts S, Halder G,
798 Hamaratoglu F. 2017. Hippo Reprograms the Transcriptional Response to Ras
799 Signaling. *Dev Cell* **42**:667-680.e4. doi:10.1016/j.devcel.2017.08.013
800 Ranganathan P, Weaver KL, Capobianco AJ. 2011. Notch signalling in solid tumours: a
801 little bit of everything but not all the time. *Nat Rev Cancer* **11**:338–351.
802 doi:10.1038/nrc3035
803 Reddy KL, Rovani MK, Wohlwill A, Katzen A, Storti RV. 2006. The Drosophila Par domain
804 protein I gene, Pdp1, is a regulator of larval growth, mitosis and endoreplication.
805 *Dev Biol* **289**:100–114. doi:10.1016/j.ydbio.2005.10.042
806 Reinke AW, Baek J, Ashenberg O, Keating AE. 2013. Networks of bZIP protein-protein
807 interactions diversified over a billion years of evolution. *Science* **340**:730–734.
808 doi:10.1126/science.1233465
809 St Johnston D, Ahringer J. 2010. Cell polarity in eggs and epithelia: parallels and
810 diversity. *Cell* **141**:757–774. doi:10.1016/j.cell.2010.05.011
811 Thurmond J, Goodman JL, Strelets VB, Attrill H, Gramates LS, Marygold SJ, Matthews BB,
812 Millburn G, Antonazzo G, Trovisco V, Kaufman TC, Calvi BR, FlyBase Consortium.
813 2019. FlyBase 2.0: the next generation. *Nucleic Acids Res* **47**:D759–D765.
814 doi:10.1093/nar/gky1003
815 Toedling J, Skylar O, Sklyar O, Krueger T, Fischer JJ, Sperling S, Huber W. 2007. Ringo--an
816 R/Bioconductor package for analyzing ChIP-chip readouts. *BMC Bioinformatics*
817 **8**:221. doi:10.1186/1471-2105-8-221
818 Toggweiler J, Willecke M, Basler K. 2016. The transcription factor Ets21C drives tumor
819 growth by cooperating with AP-1. *Sci Rep* **6**:34725. doi:10.1038/srep34725
820 Turkel N, Sahota VK, Bolden JE, Goulding KR, Doggett K, Willoughby LF, Blanco E,
821 Martin-Blanco E, Corominas M, Ellul J, Aigaki T, Richardson HE, Brumby AM.
822 2013. The BTB-zinc finger transcription factor abrupt acts as an epithelial
823 oncogene in Drosophila melanogaster through maintaining a progenitor-like cell
824 state. *PLoS Genet* **9**:e1003627. doi:10.1371/journal.pgen.1003627
825 Uhlirova M, Bohmann D. 2006. JNK- and Fos-regulated Mmp1 expression cooperates
826 with Ras to induce invasive tumors in Drosophila. *EMBO J* **25**:5294–5304.
827 doi:10.1038/sj.emboj.7601401

828 Verfaillie A, Imrichova H, Janky R, Aerts S. 2015. iRegulon and i-cisTarget:
829 Reconstructing Regulatory Networks Using Motif and Track Enrichment. *Curr*
830 *Protoc Bioinformatics* **52**:2.16.1-2.16.39. doi:10.1002/0471250953.bi0216s52
831 Wu M, Pastor-Pareja JC, Xu T. 2010. Interaction between Ras(V12) and scribbled clones
832 induces tumour growth and invasion. *Nature* **463**:545–548.
833 doi:10.1038/nature08702
834 Xia S, VanKuren NW, Chen C, Zhang L, Kemkemer C, Shao Y, Jia H, Lee U, Advani AS,
835 Gschwend A, Vibranovski MD, Chen S, Zhang YE, Long M. 2021. Genomic
836 analyses of new genes and their phenotypic effects reveal rapid evolution of
837 essential functions in Drosophila development. *PLoS Genet* **17**:e1009654.
838 doi:10.1371/journal.pgen.1009654
839 Xue B, Krishnamurthy K, Allred DC, Muthuswamy SK. 2013. Loss of Par3 promotes
840 breast cancer metastasis by compromising cell-cell cohesion. *Nat Cell Biol*
841 **15**:189–200. doi:10.1038/ncb2663
842
843

844 **FIGURE LEGENDS**

845 **Figure 1. Notch-based growth paradigms in *Drosophila* wing discs**

846 **A-D.** 3rd instar wing imaginal discs at precisely 5 days after egg-laying either wild-
847 type (WT; A), overexpressing activated Notch (N; B), mutant for *scrib* (S; C), or
848 combining overexpressed Notch and *scrib* mutation (NS; D) and marked for E-Cad
849 (blue) and Mmp1 (red). **A,B&D.** MARCM clones (positively marked by GFP; green)
850 of the indicated genotypes: expressing only GFP (A; WT), expressing Nicd & GFP (B;
851 N), and expressing Nicd & GFP and mutant for *scrib* (C; NS). **C.** Discs fully mutant
852 for *scrib*.

853 **E-F.** Differentially expressed genes as compared to WT in the different growth
854 paradigms N (green), S (red), and NS (blue) identified by RNA-Seq. This color code,
855 green for N, red for S, and blue for NS is used in all figures. **E.** Heatmap of gene
856 expressions after unsupervised clustering. **F.** Venn diagram of up-regulated and down-
857 regulated genes in N, S, and NS.

858 **G.** Enrichment diagram as measured by adjusted p-value for selected GO terms and
859 represented as bars for N (green), S (red), and NS (blue). GO terms color reflect whether
860 they are shared or specific: shared by all (black), common N&NS (dark green: mix of
861 green and blue), common S&NS (purple: mix of red and blue).

862 **H.** Venn diagram showing the domains of overlap of GO terms identified (significantly
863 enriched) in N, S, and NS.

864

865 **Figure 2. Polarity loss redirects the transcriptional output of Notch during**
866 **neoplastic growth**

867 **A.** Experimental set-up to identify the Notch Direct Targets genes (NDTs): Genes up-
868 regulated in N, S, or NS (Transcriptomic), and located within 20kb of a Su(H) binding
869 site (ChIP).

870 **B.** Venn diagram showing the NDTs overlap in N, S, and NS, showing core Notch
871 responses, but also significant condition specific NDTs.

872 **C.** Overlap of the Su(H) binding sites identified by ChIP in N, S, and NS, showing that
873 almost all S and NS Su(H) peaks are also found in N. The overlap is shown in white.
874 Numbers are slightly different because in the Su(H) peaks calling protocol, in some rare
875 cases, some peaks can be split between conditions where one peak in one condition
876 would overlap with two peaks in the other.

877 **D.** Genome Viewer snapshots of several NDTs (shown in purple) such as the NS
878 specific *Act87E* and *Wnt10* (but also *yellow-e* and *Ir87a*), the common *Ets21C*, and the
879 N/NS NDT *upd3*. For each condition, the Su(H) ChIP enrichment is shown in the upper
880 lane, and the Su(H) peaks identified are represented by the blocks underneath.
881
882 **Figure 3. Identification of potential transcriptional modules mediating N, S, and**
883 **NS growth**
884 Venn diagram of significant transcription factors (TFs) identified by iRegulon as
885 potential key mediators for the expression of the N (in the green circle), S (red circle),
886 and NS (blue circle) up-regulated genes. Fed with lists of co-regulated genes, and
887 analyzing the genomic features in the vicinity of the transcription start sites of these
888 genes, iRegulon identifies potential groups of TFs and DNA-binding factors, that are
889 enriched in the dataset of regulatory sequences, and could thus represent potential
890 mediators of the N, S, and NS transcriptomes.
891 For each condition, TFs were identified as part of "regulons" or group of TFs that could
892 potentially together regulate the expression of subsets of the transcriptome. Taking only
893 the TFs corresponding to the significant regulons identified in N, S, and NS, the shared
894 and unique potentially regulating TFs are here presented in the different colored boxes.
895 In each box, TFs were then grouped according to their molecular family (suggesting
896 pretty similar binding motifs on the DNA), and color-coded: for instance, bZIP TFs in
897 light maroon, or the nuclear receptors in brown. The molecular family color code was
898 not respected for the green and light green groups which correspond to very diverse
899 "regulons" that appear linked to epigenetic chromatin regulators/remodelers. For the
900 complete list of regulons identified in each condition, and the nature of TFs and DNA
901 binding proteins in each regulon, see Supplemental table S4).
902 Numbers in the Venn diagram represent the number of TFs identified. TFs that are also
903 NDTs and which could participate in feedforward loops are underlined (with their NDT
904 condition in parentheses). See also Figure S3 for the iRegulon analyses of the NDTs,
905 and the detailed lists of both iRegulon analyses in Supplemental Table S5.
906
907 **Figure 4. Neoplastic growth is mediated by an AP-1/Stat/Yki/Ftz-f1 module and**
908 **by a diverse network of bZIP transcription factors including Pdp1**

A-D. 3rd instar wing imaginal discs expressing *GFP*, an activated form of Notch (*Nicd*) and an RNAi for *scrib* under the control of the *Bx-Gal4* driver (dorsal wing pouch) and stained for GFP (green, white A'-D') to assess tissue overgrowth and for Mmp1 (red, white A''-D'') to assess tissue invasiveness. Discs also expressed under *Bx-Gal4* control the either *UAS Bsk DN* (B) or the indicated RNAi constructs: *w[HMS00045]* (A; Ctrl), *yki[HMS00041]* (C), *Pdp1[HMS02030]* (D). Representative discs are shown.

E. Quantification of the overgrowth of the GFP territory in the indicated genotypes. Results are shown as violin plots of total GFP area measured in arbitrary pixels. In grey are represented the controls for each experiment. Statistical tests: ANOVA (left and middle graphs) or unpaired two tailed t-test (right graph); n.s. non significant; * $p<0.05$; ** $p<0.01$; *** $p<0.001$; **** $p<0.0001$.

For more details of RNAi lines either from the TRiP collection (labelled with trip superscript) or from the Vienna collection (labelled with KK superscript) are provided in supplemental information.

F. Quantification of the Mmp1 intensity in the indicated genotypes. Results are shown as percentage where discs were classified to fall in three categories: High Mmp1 staining intensity (red, similar to that shown in A''), Low Mmp1 staining intensity (blue, similar to that shown in D''), No Mmp1 staining (light blue, similar to that shown in B''). Statistical test: chi-square test for trend or Fisher's exact test; * $p<0.05$.

G. Feedforward model of the cooperation between Notch and polarity loss during wing imaginal disc neoplastic growth.

E-G. The Pdp1, Ets21C, and Ftz-f1 NDTs are highlighted with an underline.

Logeay et al. Figure 1

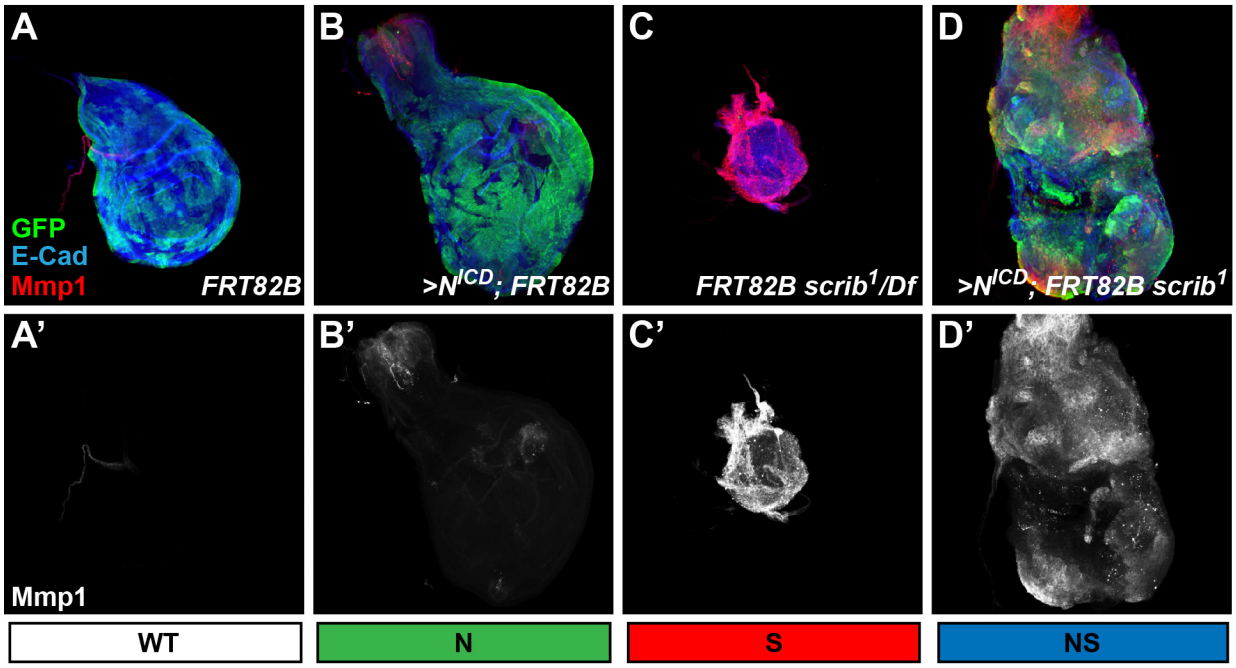

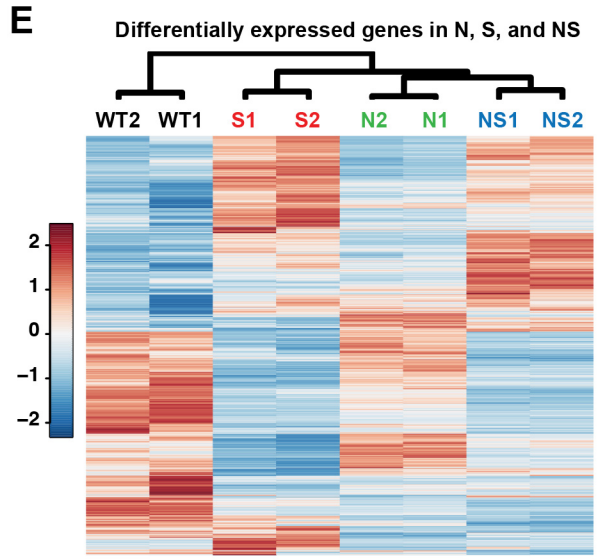

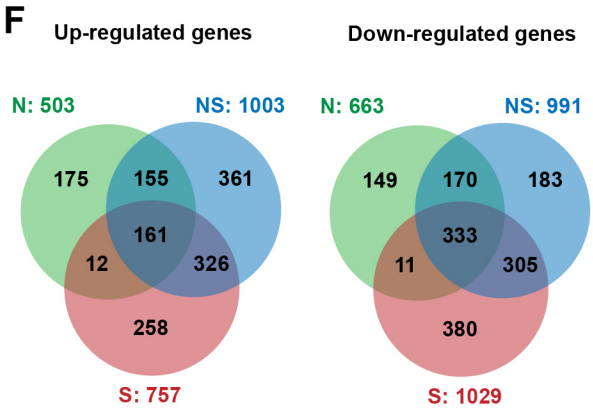

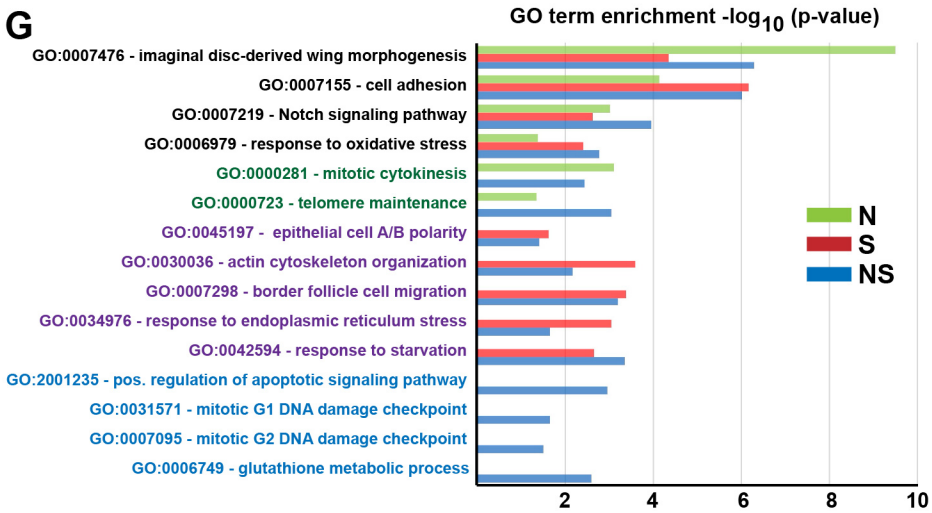

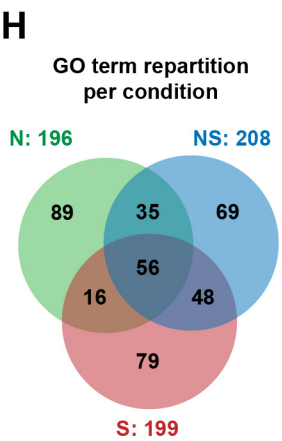

Logeay et al. Figure 2

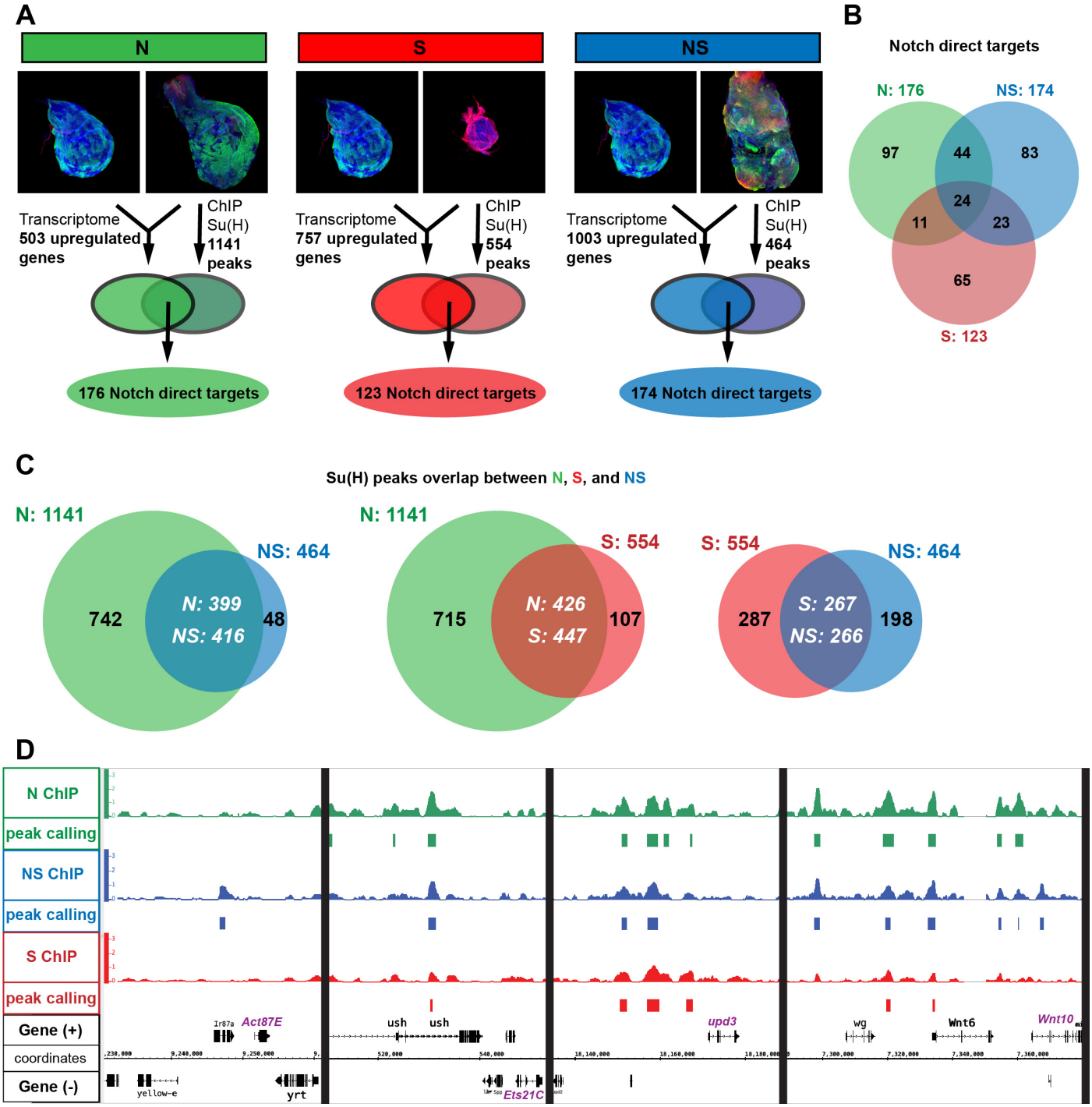

Logeay et al. Figure 3

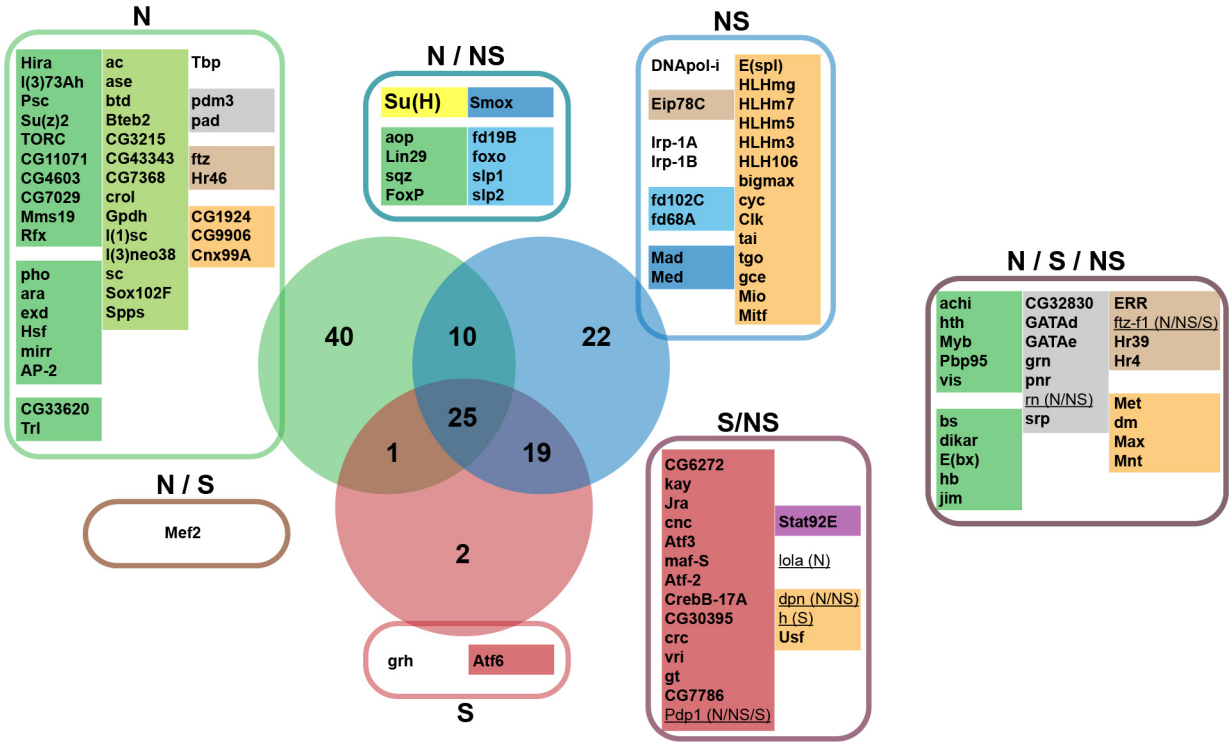

Logeay et al. Figure 4

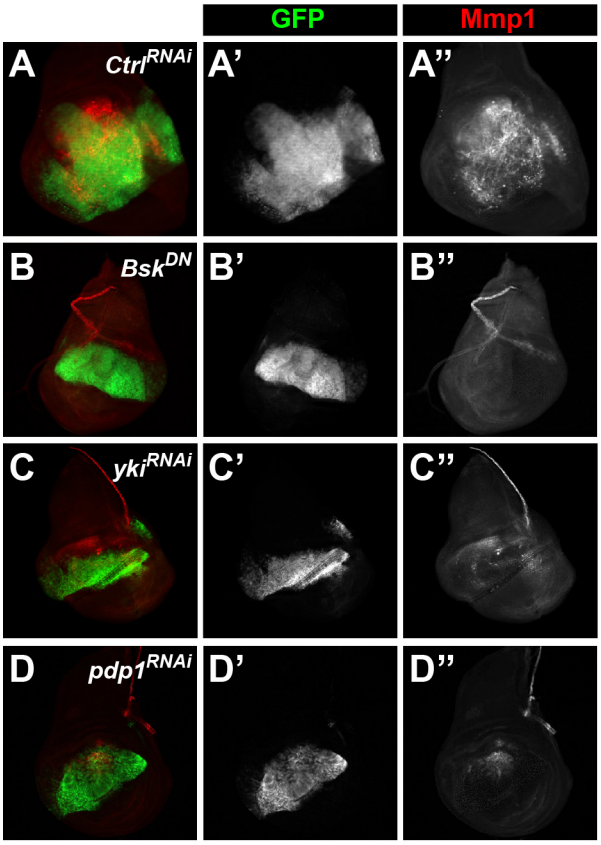

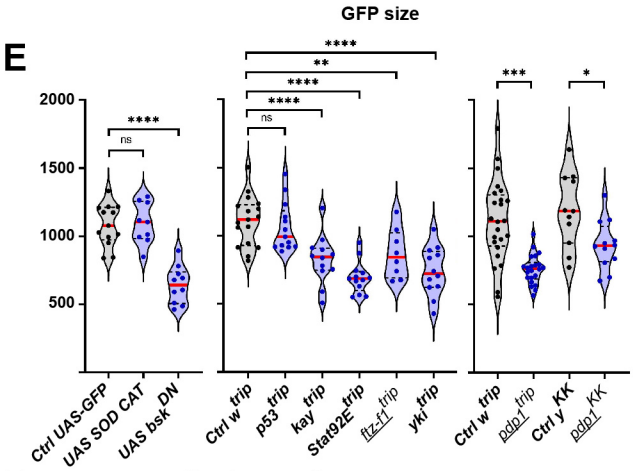

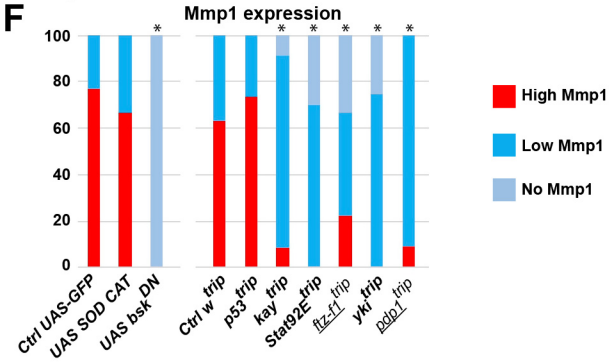

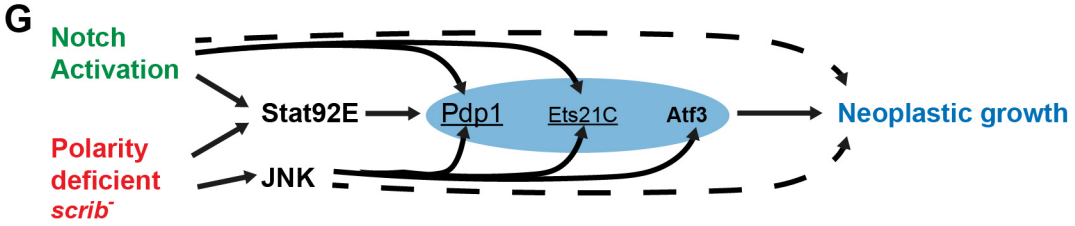

SUPPLEMENTAL INFORMATION

SUPPLEMENTAL MATERIAL AND METHODS

Drosophila genetics

Driver lines were *Bx-Gal4* (wing disc pouch), *Dpp-Gal4*, and *Ptc-Gal4* (both wing disc antero-posterior boundary). Overexpression lines were *UAS Nicd* (made by the Bray lab), *UAS GFP:Act87E [7-6]* BL#9249, and *UAS Pdp1.T* BL#78087.

Overexpression lines tested in the *Bx-Gal4, UAS GFP;; UAS Nicd, UAS scribHMS01490* screen were *UAS GFP*, *UAS bskK53R [20.1a]* BL#9311, and *UAS SOD CAT* (gift from P. Leopold). RNAi lines used are listed in the table below with an indication of the labels used in Fig. 4E&F. TRiP collection lines have a stock BL#, and Vienna collection lines have a stock v#. While performing the *Bx>NS* modifier experiments, we used controls originating from the same collection: *RNAi white* for TRiP lines, and *RNAi yellow* for Vienna KK lines.

Gene	RNAi ID	Stock #
Act87E	HMS02488	BL#42642
Act87E	KK111781	v#102480
cdi	KK100725	v#109409
CG7059	GD10763	v#21651
CG13850	KK104804	v#100863
CG13857	GD6226	v#44061
CG18596	KK104660	v#108183
ftz-f1	HMS00019	BL#33625
Ir87a	HMJ22848	BL#60476
Ir87a	KK106593	v#100667
kay	HMS00254	BL#33379
p53	HMS02286	BL#41720
Pdp1	HMS02030	BL#40863
Pdp1	KK109014	v#110551
REG	KK102083	v#110156
stat92E	HMS00035	BL#33637

vito	KK111866	v#102513
w	HMS00045	BL#33644
y	KK104196	v#106068
yellow-e	HMC06250	BL#65970
yellow-e	KK106243	v#100926
yellow-e3	KK106158	v#105879
yki	HMS00041	BL#34067

Primers

qPCR primers:

Act5C_F: GAGCGCGGTTACTCTTTCAC

Act5C_R: ACTTCTCCAACGAGGAGCTG

Act87E_F: GTCCACCGCAAGTGCTTCTA

Act87E_R: TTTCTTTGGATGGCAGGGCA

Atf3_F: CAGCATGGCAACATTGGGAC

Atf3_R: ATGAAGGCAGTGGCTGAGTC

Diap1_F: CAGCCACACGCATCTTCAAC

Diap1_R: ACTTTGTCACAGAGGAGGCG

E2f1_F: ACAGAATCCTCGCCTCCAAC

E2f1_R: GACTGCTGCCGTAGCCTATT

Ets21C_F: CTGCTCGCTGATTCGTCCAA

Ets21C_R: TAGGCATACCGCTTTCCGTG

ftz-f1_F: ATTCCTGGTCGGACATGCTT

ftz-f1_R: TTCATGCAGACATAGTCGCCC

mxc_F: ACTAGAGGAGGAGCAGCGAA

mxc_R: CTAGTGGACAGCGGCGTATT

p38a_F: TACGGACAGGTGTCAAAGGC

p38a_R: CAGCGATCCATTAGCGGGAT

p53_F: TGCGTGTGTTCCTTTGCTTC

p53_R: GTTCAGGGGGACTACAACGG

puc_F: ATTGACCTCGCCGCCAATTA

puc_R: ATTCCGCTTGAACAGAGCCA

42 sd_F: AGGGTCCACAGAATGCGTTT
43 sd_R: TCGCTTTCCACCTTCTCCAC
44 Sdr_F: CGCTCCCTCAATCCCAAAGT
45 Sdr_R: ACAACGTCCATCAGCCAGTT
46 Ser_F: GCACGAATCTCTGGTGTGGA
47 Ser_R: TAGATTTGGCTGGCAGTCGG
48 wg_F: GCAGTCTGGTCTGGTCTACG
49 wg_R: ATTGTGCGGGTTCAGTTGGA
50 Wnt10_F: AATGGCATCGGTGGAACTGT
51 Wnt10_R: CAGCGTCTTGCGATTGATGG
52
53 qChIP primers:
54 E(spl)mβ_F: AAGTCGGAGCTTTGAATGAG
55 E(spl)mβ_R: CAAGTCATTTTATTGCCCTCAC
56 E(spl)m5_F: GTTTCCGCAGGTCCAGTTAC
57 E(spl)m5_R: GTTTGATGTTCACGCTGCTG
58 white_F: CGAAGGACGTTGACACATTG
59 white_R: GAATTGCCGCTTTTTCTCAC
60 DDC_F: AAGTGGGATTTGCCAGTGAC
61 DDC_R: TGCTGGTGAACTTTGACTGC
62 CG42808_F: CTCGTTAAGAGCAACTGCGA
63 CG42808_R: GTGAGAACTCCGAATCGAGG
64 CG6191_F: CGAAAAATGCGGACGATTCC
65 CG6191_R: CCCACCAATCTAGGGTTTCA
66 Ilp8_F: TCATCTCCGGTGTCTGACTT
67 Ilp8_R: AAAGAATTGGCTGCGGAAGA
68
69
70 **SUPPLEMENTAL FIGURE LEGENDS**
71 **Figure S1. Features of the Notch Direct Targets (NDTs) in N, S, and NS (relates to**
72 **Fig. 3)**
73 **A.** Semi-quantitative RT-PCR of the indicated genes represented as fold change
74 compared to WT (grey) in the different N (green), S (red), and NS (blue) growth

75 paradigms and normalized to *Atc5C* expression. Biological triplicates, standard error to
76 the mean (s.e.m.) is shown. ANOVA statistical test, * $p<0.05$.
77 **B.** Heatmaps for the expression of the different NDTs in WT, N, S, and NS. From left
78 to right are presented the N, S, NS, and finally All NDTs, highlighting that NDTs could
79 be transcriptionally up-regulated in more than in one condition.
80 **C.** Genome browser view of the whole left arm of the 2nd chromosome, and showing
81 the Su(H) ChIP enrichment (upper rows) and the intervals called as Su(H) peaks (lower
82 rows) in N (green), NS (blue), and S (red). Note the higher number of peaks in N, and
83 the rarity of NS, or S peaks not found in N.
84
85 **Figure S2. Act87E promotes Mmp1 expression and cell delamination.**
86 **A-B.** GFP:Act87E overexpressed together with activated Notch (Nicd) under the
87 control of the *Ptc-Gal4* driver (antero/posterior boundary cells in green, A'&B'),
88 promotes the expression of the Dcp-1 caspase (red, A''), and the metalloprotease Mmp1
89 (red, B''). Similar results were obtained for the sole overexpression of GFP:Act87E
90 (without Nicd). DAPI (blue, A''') or E-Cad (blue, B''') mark all wing disc cells. (A)
91 Whole wing disc. (B) Detail of the overgrowing wing pouch (magnification in B is
92 twice that in A).
93
94
95 **Figure S3. Identification of potential transcriptional modules mediating N, S, and**
96 **NS growth (relates to Fig. 3)**
97 Venn diagram of significant transcription factors (TFs) identified by iRegulon as
98 potential key mediators for the expression of the N (in the green circle), S (red circle),
99 and NS (blue circle) Notch Direct Target (NDT) genes. Fed with lists of co-regulated
100 genes, and analyzing the genomic features in the vicinity of the transcription start sites
101 of these genes, iRegulon identifies potential groups of TFs and DNA-binding factors,
102 that are enriched in the dataset of regulatory sequences, and could thus represent
103 potential mediators regulating the expression of NDT genes in N, S, and NS.
104 For each condition, TFs were identified as part of "regulons" or group of TFs that could
105 potentially together regulate the expression of subsets of the transcriptome. Taking only
106 the TFs corresponding to the significant regulons identified in N, S, and NS, the shared
107 and unique potentially regulating TFs are here presented in the different colored boxes.

108 In each box, TFs were then grouped according to their molecular family (suggesting
109 pretty similar binding motifs on the DNA), and color-coded: for instance, bZIP TFs in
110 light maroon, or the nuclear receptors in brown. The molecular family color code was
111 not respected for the green groups which correspond to very diverse "regulons" that
112 appear linked to epigenetic chromatin regulators/remodelers. For the complete list of
113 regulons identified in each condition, and the nature of TFs and DNA binding proteins
114 in each regulon, see Supplemental table S5).
115 Numbers in the Venn diagram represent the number of TFs identified. TFs that are also
116 NDTs and which could participate in feedforward loops are underlined (with their NDT
117 condition in parentheses).
118
119 **Figure S4. Pdp1 is a direct Notch target (relates to Fig. 4)**
120 **A.** Genome browser view of the *Pdp1* locus, and showing the Su(H) ChIP enrichment
121 (upper rows) and the intervals called as Su(H) peaks (lower rows) in N (green), NS
122 (blue), and S (red).
123 **B-E.** Pdp1 overexpression causes Mmp1 expression. GFP alone (B) or in combination
124 with *Pdp1* (C), with *Nicd* (D), or with *Nicd & Pdp1* (E) was overexpressed using the
125 *Dpp-Gal4* driver. Higher magnification corresponding to the yellow dashed boxes show
126 GFP in green (B'-E') and Mmp1 in red (B''-E''). E-Cad used as landmark is shown in
127 blue (B-E). Pdp1 overexpression resulted in Mmp1 positive cells extending anteriorly
128 (C). This was enhanced when combined with Nicd (E). Representative discs shown (out
129 of 18 imaged discs from 3 experiments).
130 **(E)** Mmp1 expression is found in the *Pdp1&Nicd* overexpressing cells (GFP positive
131 under the influence of the *Dpp-Gal4* driver), but also in non-expressing cells (non-
132 autonomous, yellow arrowhead).
133
134
135 **SUPPLEMENTAL TABLES**
136 **Table S1.** Differentially expressed genes in N, S, and NS identified by DESeq (related
137 to Fig. 1). Columns are:
138 FBgn_ID: Unique FlyBase gene ID
139 Symbol: Current FlyBase gene symbol
140 qval: adjusted p-value for multiple testing

141 logFC: log2 of the Fold Change “Condition N, S, or NS” / “Control WT”

142

143 **Table S2.** Su(H) ChIP enrichment peaks coordinates in N, S, and NS (related to Fig.
144 3). Columns are:
145 Exp: N, S, or NS
146 Chr: Chromosome arm
147 MIN: smallest peak coordinate
148 MAX: biggest peak coordinate

149

150 **Table S3.** All Notch Direct Targets (NDTs) ordered by genomic position. This table
151 includes an indication whether the genes are transcriptionally upregulated or have a
152 Su(H) peak in the vicinity in each N, S, and NS condition. Columns are:
153 N/NS/S: NDT in the corresponding condition
154 Type: NDT in different conditions.
155 FBgn_ID: Unique FlyBase gene ID
156 SYMBOL: Current FlyBase gene symbol
157 K_ARM: Chromosome arm location of the gene
158 MIN (gene pos): smallest gene coordinate
159 MAX (gene pos): biggest gene coordinate
160 STRAND: +1 or -1
161 N Fold: Log2 Fold Change in gene expression N/WT (n.s. not significant)
162 N ChIP: Su(H) ChIP enrichment peak within 20kb in N (green yes, red no)
163 NS Fold: Log2 Fold Change in gene expression NS/WT (n.s. not significant)
164 NS ChIP: Su(H) ChIP enrichment peak within 20kb in NS (green yes, red no)
165 S Fold: Log2 Fold Change in gene expression S/WT (n.s. not significant)
166 S ChIP: Su(H) ChIP enrichment peak within 20kb in S (green yes, red no)

167

168 **Table S4.** Curated iRegulon analyses of the significantly upregulated genes in N, S,
169 and NS (related to Fig. 3). Analyses were performed using the 6K-PWM and 10kb
170 upstream and downstream set-ups.

171

172 **Table S5.** Curated iRegulon analyses of the Notch Direct Targets in N, S, and NS
173 (related to Fig. S2). Analyses were performed using the 6K-PWM and 10kb upstream
174 and downstream set-ups.

Logeay et al. Figure S1

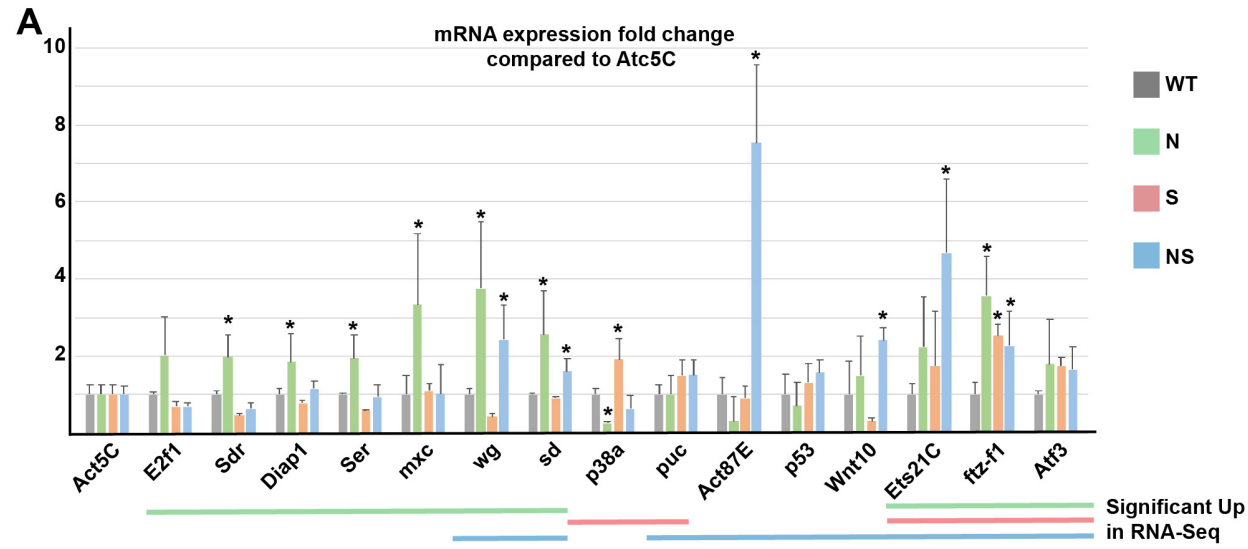

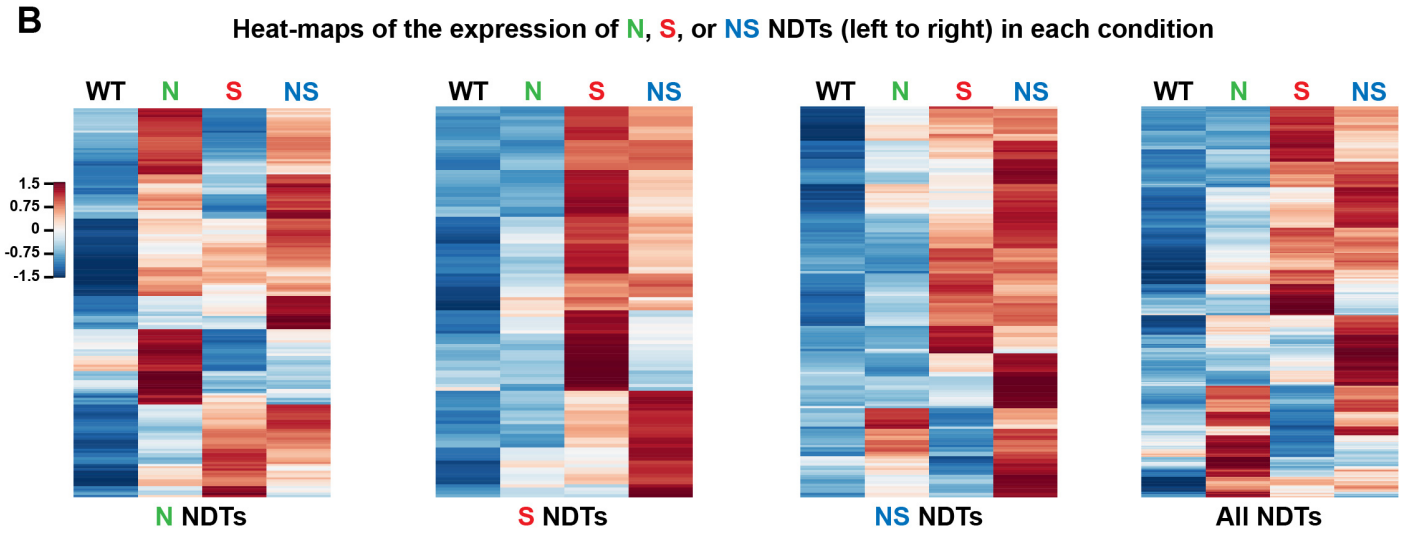

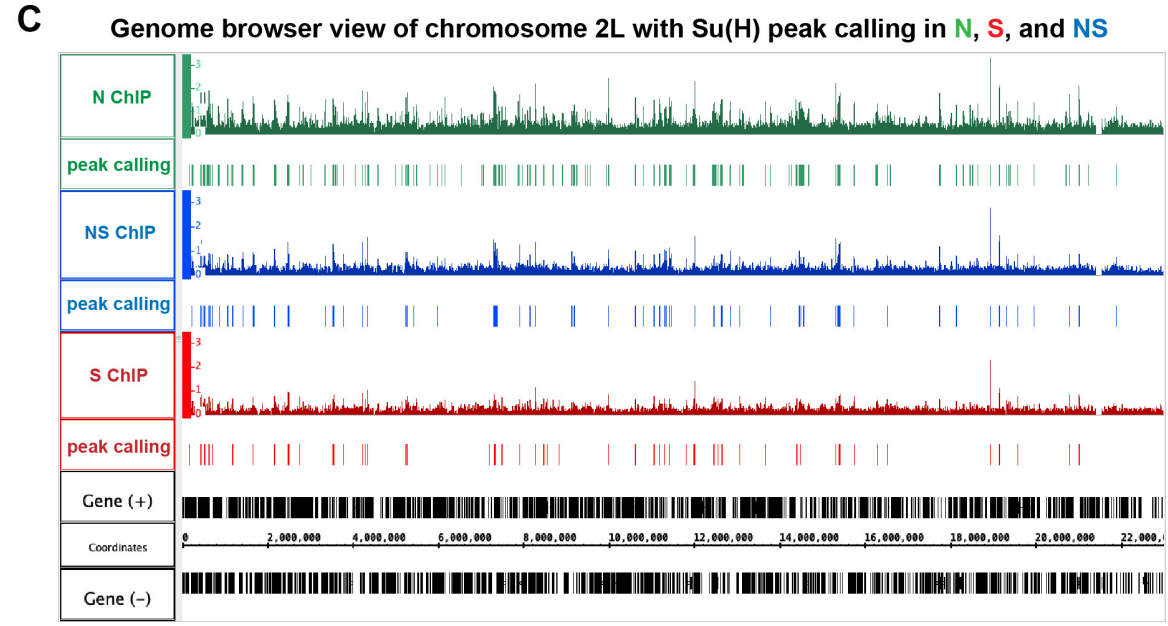

Logeay et al. Figure S2

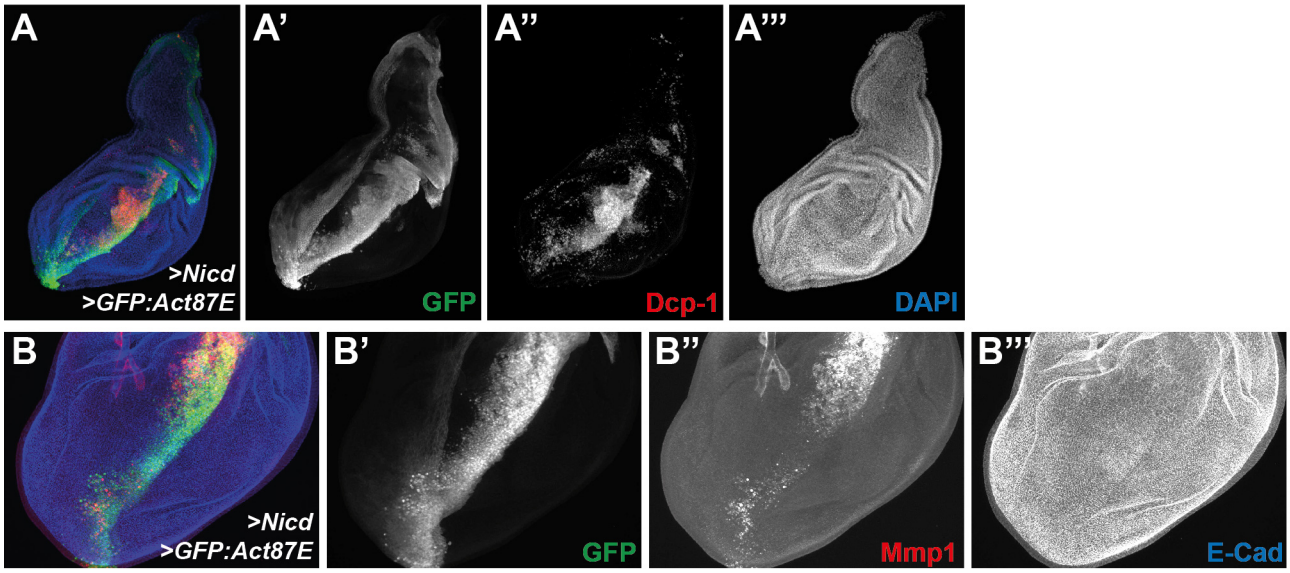

Logeay et al. Figure S3

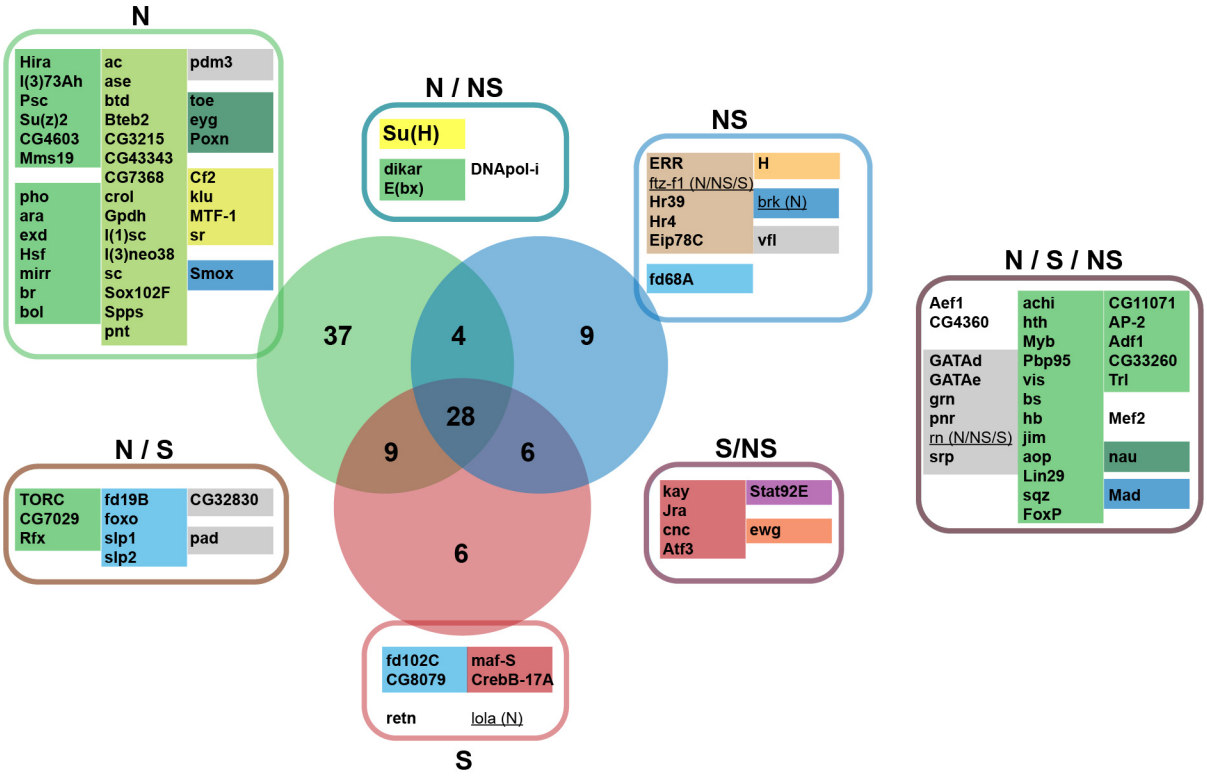
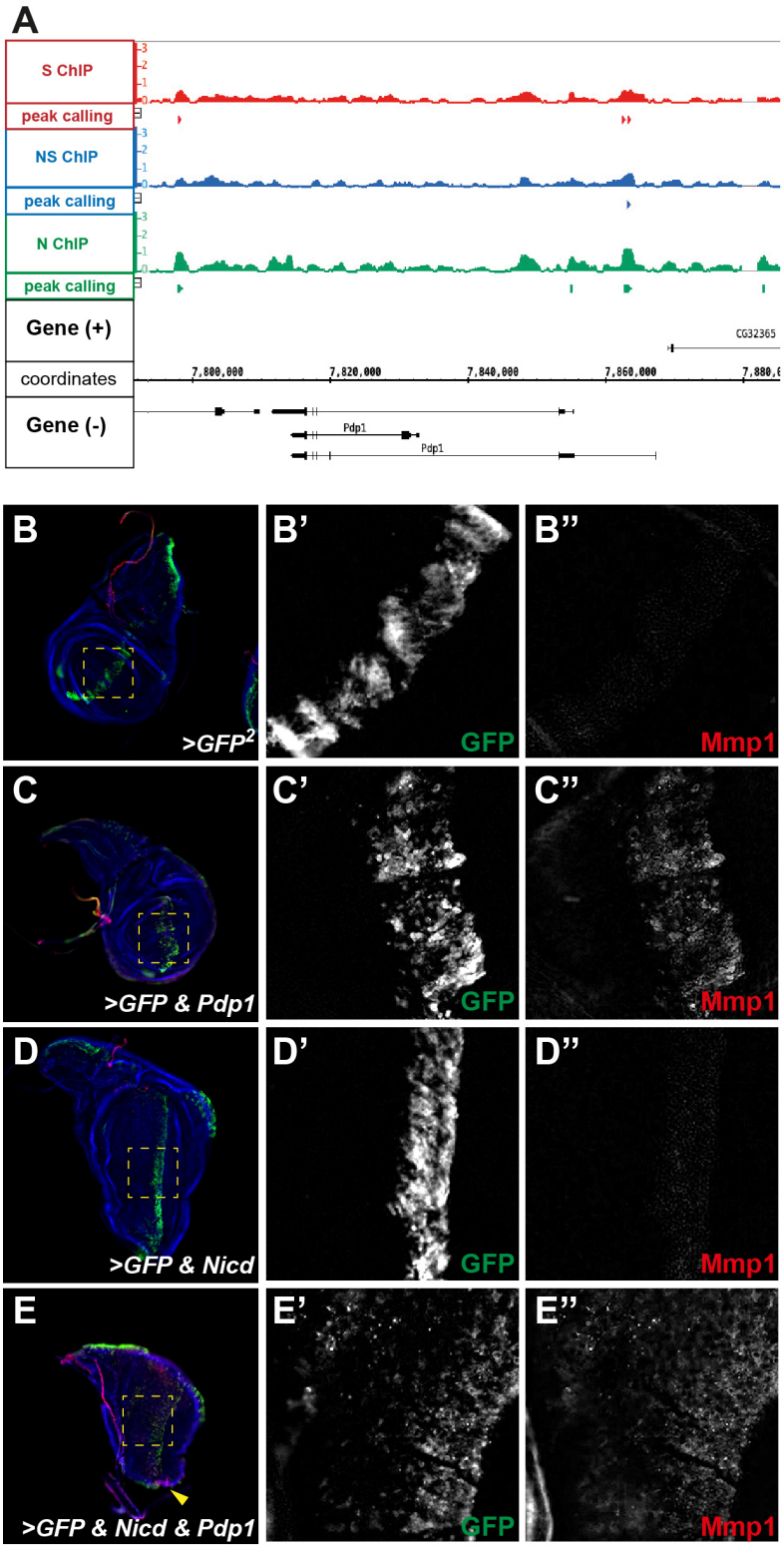
Logeay et al. Figure S4